Inorg. Chem. **2005**, *44*, 1713–1727

Synthetic Control of Excited-State Properties in Cyclometalated Ir(III) Complexes Using Ancillary Ligands

Jian Li,[†] Peter I. Djurovich,[†] Bert D. Alleyne,[†] Muhammed Yousufuddin,[†] Nam N. Ho,[†] J. Christopher Thomas,[‡] Jonas C. Peters,[‡] Robert Bau,[†] and Mark E. Thompson*,[†]

University of Southern California, Department of Chemistry, Los Angeles, California 90089, and Division of Chemistry and Chemical Engineering, Arnold and Mabel Beckman Laboratories of Chemical Synthesis, California Institute of Technology, Pasadena, California 91125

Received October 7, 2004

The synthesis and photophysical characterization of a series of (N,C$^{2'}$-(2-*para*-tolylpyridyl))$_2$Ir(LL′) [(*tpy*)$_2$Ir(LL′)] (LL′ = 2,4-pentanedionato (acac), bis(pyrazolyl)borate ligands and their analogues, diphosphine chelates and *tert*-butylisocyanide (CN-*t*-Bu)) are reported. A smaller series of [(*dfppy*)$_2$Ir(LL′)] (*dfppy* = N,C$^{2'}$-2-(4′,6′-difluorophenyl)-pyridyl) complexes were also examined along with two previously reported compounds, (*ppy*)$_2$Ir(CN)$_2^-$ and (*ppy*)$_2$Ir(NCS)$_2^-$ (*ppy* = N,C$^{2'}$-2-phenylpyridyl). The (*tpy*)$_2$Ir(PPh$_2$CH$_2$)$_2$BPh$_2$ and [(*tpy*)$_2$Ir(CN-*t*-Bu)$_2$](CF$_3$SO$_3$) complexes have been structurally characterized by X-ray crystallography. The Ir–C$_{aryl}$ bond lengths in (*tpy*)$_2$Ir(CN-*t*-Bu)$_2^+$ (2.047(5) and 2.072(5) Å) and (*tpy*)$_2$Ir(PPh$_2$CH$_2$)$_2$BPh$_2$ (2.047(9) and 2.057(9) Å) are longer than their counterparts in (*tpy*)$_2$Ir(acac) (1.982(6) and 1.985(7) Å). Density functional theory calculations carried out on (*ppy*)$_2$Ir(CN-Me)$_2^+$ show that the highest occupied molecular orbital (HOMO) consists of a mixture of phenyl-π and Ir-d orbitals, while the lowest unoccupied molecular orbital is localized primarily on the pyridyl-π orbitals. Electrochemical analysis of the (*tpy*)$_2$Ir(LL′) complexes shows that the reduction potentials are largely unaffected by variation in the ancillary ligand, whereas the oxidation potentials vary over a much wider range (as much as 400 mV between two different LL′ ligands). Spectroscopic analysis of the cyclometalated Ir complexes reveals that the lowest energy excited state (T$_1$) is a triplet ligand-centered state (^{3}LC) on the cyclometalating ligand admixed with ^{1}MLCT (MLCT = metal-to-ligand charge-transfer) character. The different ancillary ligands alter the ^{1}MLCT state energy mainly by changing the HOMO energy. Destabilization of the ^{1}MLCT state results in less ^{1}MLCT character mixed into the T$_1$ state, which in turn leads to an increase in the emission energy. The increase in emission energy leads to a linear decrease in ln(k_{nr}) (k_{nr} = nonradiative decay rate). Decreased ^{1}MLCT character in the T$_1$ state also increases the Huang–Rhys factors in the emission spectra, decreases the extinction coefficient of the T$_1$ transition, and consequently decreases the radiative decay rates (k_r). Overall, the luminescence quantum yields decline with increasing emission energies. A linear dependence of the radiative decay rate (k_r) or extinction coefficient (ϵ) on $(1/\Delta E)^2$ has been demonstrated, where ΔE is the energy difference between the ^{1}MLCT and ^{3}LC transitions. A value of 200 cm^{-1} for the spin–orbital coupling matrix element $\langle ^3\text{LC}|H_{SO}|^1\text{MLCT}\rangle$ of the (*tpy*)$_2$Ir(LL′) complexes can be deduced from this linear relationship. The (*fppy*)$_2$Ir(LL′) complexes with corresponding ancillary ligands display similar trends in excited-state properties.

Introduction

During the last two decades, luminescent cyclometalated Ir(III) complexes have exhibited an enormous potential for a range of photonic applications. For example, these Ir complexes can be used as emissive dopants in organic light emitting devices (OLEDs),[1,2] sensitizers for outer-sphere

* To whom correspondence should be addressed. E-mail: met@usc.edu.
[†] University of Southern California.
[‡] California Institute of Technology.

(1) (a) Baldo, M. A.; O'Brien, D. F.; You, Y.; Shoustikov, A.; Sibley, S.; Thompson, M. E.; Forrest, S. R. *Nature* **1998**, *395*, 151. (b) Baldo, M. A.; Lamansky, S.; Burrows, P. E.; Thompson, M. E.; Forrest, S. R. *Appl. Phys. Lett.* **1999**, *75*, 4. (c) Thompson, M. E.; Burrows, P. E.; Forrest, S. R. *Curr. Opin. Solid State Mater. Sci.* **1999**, *4*, 369. (d) Baldo, M. A.; Thompson, M. E.; Forrest, S. R. *Nature* **2000**, *403*, 750.

10.1021/ic048599h CCC: $30.25
Published on Web 02/12/2005

electron-transfer reactions,[3,4] photocatalysts for CO_2 reduction,[5,6] photooxidants and singlet oxygen sensitizers,[7] and biological labeling reagents.[8] Since the optical properties and related uses of the cyclometalated Ir complexes are strongly dependent on the characteristics of their ground and lowest excited states, it becomes desirable to better understand the interactions between these states and thus determine how to systematically alter the photophysical properties by appropriate ligand design.

Several research groups have established that luminescence from cyclometalated Ir(III) and Rh(III) complexes originates from a lowest triplet excited (T_1) state that is ligand centered (^{3}LC) with singlet metal-to-ligand charge-transfer (^{1}MLCT) character mixed in through spin−orbit coupling.[9−13] The admixture of ^{1}MLCT character into what is principally a ^{3}LC state has dramatic effects on the optical properties of those complexes,[9] including a large decrease in the luminescence lifetimes and the appearance of metal−ligand vibrational sidebands in absorption and luminescence spectra.[13,14] In addition, since the lowest excited state is ^{3}LC-dominant, employing different cyclometalating ligands enables the excited-state energy of Ir complexes to be varied over a wide spectral range. Thus, through careful selection of ligands, it is possible to "tune" the emission color from red to blue.[15−22] Interesting questions still remain regarding the luminescent properties of the cyclometalated Ir complexes; e.g., to what extent can the admixture of ^{3}LC and ^{1}MLCT states be controlled, and how does a change in the admixture influence the excited-state properties of Ir complexes? Several studies have investigated the use of electron donating and withdrawing groups on the cyclometalating ligand in order to raise or lower the MLCT emission energy.[14] However, the relative positions between ^{1}MLCT and ^{3}LC state energies will not systematically vary by modifying the cyclometalating ligand, since altering the cyclometalate will influence both state energies simultaneously.[14]

To investigate the interactions between ^{1}MLCT and ^{3}LC states on the excited-state properties of Ir cyclometalates, we have prepared a series of bis-cyclometalated Ir(III) complexes having the same cyclometalating ligand, either N,C$^{2'}$-(2′-*para*-tolylpyridyl) (*tpy*) or N,C$^{2'}$-2-(4′,6′-difluorophenyl)pyridyl (*dfppy*), and different ancillary ligands (LL′). Two recently reported anionic complexes with N,C$^{2'}$-2-phenylpyridyl (*ppy*) ligands were also examined.[18] The structures and abbreviations for the cyclometalated complexes reported here, numbered **1**−**12** for $(tpy)_2$Ir(LL′) and **13**−**14** for $(ppy)_2$Ir(LL′), are listed in Figure 1, where *C*∧*N* is a general abbreviation for both cyclometalating ligands and LL′ is the ancillary ligand. Some selected $(dfppy)_2$Ir(LL′) complexes were also synthesized with corresponding ancillary ligands. The ancillary ligands form air stable complexes[23−27] and were also chosen to be "nonchromophoric", i.e., to have sufficiently high singlet and triplet energies such that the excited-state properties are dominated by the "$(C\wedge N)_2$Ir" fragment. Therefore, the energy of the ^{3}LC state is expected to be relatively constant for all related $(C\wedge N)_2$Ir(LL′) complexes while the energy of ^{1}MLCT states can be altered by varying the electron withdrawing/donating effects of the ancillary ligand. Although the influence of various nonchromophoric ligands on the excited states of

(2) (a) Lamansky, S.; Djurovich, P. I.; Abdel-Razzaq, F.; Garon, S.; Murphy, D. L.; Thompson, M. E. *J. Appl. Phys.* **2002**, *92*, 1570. (b) Chen, F. C.; Yang, Y.; Thompson, M. E.; Kido, J. *Appl. Phys. Lett.* **2002**, *80*, 2308. (c) Markham, J. P. J.; Lo, S.-C.; Magennis, S. W.; Burn, P. L.; Samuel, I. D. W. *Appl. Phys. Lett.* **2002**, *80*, 2645. (d) Zhu, W.; Mo, Y.; Yuan, M.; Yang, W.; Cao, Y. *Appl. Phys. Lett.* **2002**, *80*, 2045.

(3) (a) Sutin, N. *Acc. Chem. Res.* **1968**, *1*, 225. (b) Meyer, T. J. *Acc. Chem. Res.* **1978**, *11*, 94.

(4) Schmid, B.; Garces, F. O.; Watts, R. J. *Inorg. Chem.* **1994**, *32*, 9.

(5) (a) Belmore, K. A.; Vanderpool, R. A.; Tsai, J. C.; Khan, M. A.; Nicholas, K. M. *J. Am. Chem. Soc.* **1988**, *110*, 2004. (b) Silavwe, N. D.; Goldman, A. S.; Ritter, R.; Tyler, D. R. *Inorg. Chem.* **1989**, *28*, 1231.

(6) King, K. A.; Spellane, P. J.; Watts, R. J. *J. Am. Chem. Soc*. **1985**, *107*, 1431.

(7) (a) Demas, J. N.; Harris, E. W.; McBride, R. P. *J. Am. Chem. Soc*. **1977**, *99*, 3547. (b) Demas, J. N.; Harris, E. W.; Flynn, C. M.; Diemente, J. D. *J. Am. Chem. Soc.* **1975**, *97*, 3838. (c) Gao, R.; Ho, D. G.; Hernandez, B.; Selke, M.; Murphy, D.; Djurovich, P. I.; Thompson, M. E. *J. Am. Chem. Soc.* **2002**, *124*, 14828.

(8) Lo, K. K.-W.; Chung, C.-K.; Lee, T. K.-M.; Lui, L.-K.; Tsang, K. H.-K.; Zhu, N. *Inorg. Chem.* **2003**, *42*, 6886.

(9) Colombo, M. G.; Güdel, H. U. *Inorg. Chem.* **1993**, *32*, 3081.

(10) Strouse, G. F.; Güdel, H. U.; Bertolasi, V.; Ferretti, V. *Inorg. Chem.* **1995**, *34*, 5578.

(11) Lever, A. P. B. *Inorganic Electronic Spectroscopy*, 2nd ed.: Elsevier: New York, 1984; pp 174−178.

(12) (a) Wiedenhofer, H.; Schützenmeier, S.; von Zelewsky, A.; Yersin, H. *J. Phys. Chem.* **1995**, *99*, 13385. (b) Schmidt, J.; Wiedenhofer, H.; von Zelewsky, A.; Yersin, H. *J. Phys. Chem.* **1995**, *99*, 226.

(13) Yersin, H.; Donges, D. *Top. Curr. Chem.* **2001**, *214*, 81−186.

(14) Vanhelmont, F. W. M.; Güdel, H. U.; Förtsch, M.; Bürgi, H.-B. *Inorg. Chem.* **1997**, *36*, 5512.

(15) Lamansky, S.; Djurovich, P.; Murphy, D.; Abdel-Razzaq, F.; Kwong, R.; Tsyba, I.; Bortz, M.; Mui, B.; Bau, R.; Thompson, M. E. *Inorg. Chem.* **2001**, *40*, 1704.

(16) Tamayo, A. B.; Alleyne, B. D.; Djurovich, P. I.; Lamansky, S.; Tsyba, I.; Ho, N. H.; Bau, R.; Thompson, M. E. *J. Am. Chem. Soc.* **2003**, *125*, 7377.

(17) (a) Grushin, V. V.; Herron, N.; LeCloux, D. D.; Marshall, W. J.; Petrov, V. A.; Wang, Y. *Chem. Commun.* **2001**, (16), 1494. (b) Wang, Y.; Herron, N.; Grushin, V. V.; LeCloux, D.; Petrov, V. *Appl. Phys. Lett.* **2001**, *79*, 449.

(18) Nazeeruddin, Md. K.; Humphry-Baker, R.; Berner, D.; Rivier, S.; Zuppiroli, L.; Graetzel, M. *J. Am. Chem. Soc.* **2003**, *125*, 8790.

(19) Brooks, J.; Babayan, Y.; Lamansky, S.; Djurovich, P. I.; Tsyba, I.; Bau, R.; Thompson, M. E. *Inorg. Chem.* **2002**, *41*, 3055.

(20) Tsuboyama, A.; Iwawaki, H.; Furugori, M.; Mukaide, T.; Kamatani, J.; Igawa, S.; Moriyama, T.; Miura, S.; Takiguchi, T.; Okada, S.; Hoshino, M.; Ueno, K. *J. Am. Chem. Soc.* **2003**, *125*, 12971.

(21) (a) Finkenzeller, W. J.; Yersin, H. *Chem. Phys. Lett.* **2003**, *377*, 299. (b) Finkenzeller, W. J.; Stoessel, P.; Yersin, H. *Chem. Phys. Lett.* **2004**, *397*, 289.

(22) Adachi, C.; Kwong, R. C.; Djurovich, P.; Admovich, V.; Baldo, M. A.; Thompson, M. E.; Forrest, S. R. *Appl. Phys. Lett*. **2001**, *79*, 2082.

(23) Trofimenko, S. *J. Am. Chem. Soc.* **1967**, *89*, 3170.

(24) (a) Breakell, K. R.; Patmore, D. J.; Storr, A. *J. Chem. Soc., Dalton Trans.* **1975**, 749. (b) Komorowski, L.; Maringgele, W.; Meller, A.; Niedenzu, K.; Serwatowski, J. *Inorg. Chem.* **1990**, *29*, 3845.

(25) (a) Tellers, D. M.; Bergman, R. G. *J. Am. Chem. Soc.* **2001**, *123*, 11508. (b) Tellers, D. M.; Bergman, R. G. *J. Am. Chem. Soc.* **2000**, *122*, 954. (c) Wiley: J. S.; Heinekey, D. M. *Inorg. Chem.* **2002**, *41*, 4961. (d) Gutierrez-Puebla, E.; Monge, A.; Paneque, M.; Poveda, M. L.; Salazar, V.; Carmona, E. *J. Am. Chem. Soc.* **1999**, *121*, 248. (e) Tellers, D. M.; Bergman, R. G. *Organometallics* **2001**, *20*, 4819.

(26) (a) Trofimenko, S. *Chem. Rev.* **1993**, *93*, 943. (b) Vicente, J.; Chicote, M. T.; Guerrero, R.; Herber, U.; Bautista, D. *Inorg. Chem.* **2002**, *41*, 1870. (c) Paulo, A.; Domingos, A.; Santos, I. *Inorg. Chem.* **1996**, *35*, 1798. (d) Kitano, T.; Sohrin, Y.; Hata, Y.; Kawakami, H.; Hori, T.; Ueda, K. *J. Chem. Soc., Dalton Trans.* **2001**, 3564. (e) Shi, X.; Ishihara, T.; Yamanaka, H.; Gupton, J. T. *Tetrahedron Lett.* **1995**, *36*, 1527. (f) Yamanaka, H.; Takekawa, T.; Morita, K.; Ishihara, T.; Gupton, J. T. *Tetrahedron Lett.* **1996**, *37*, 1829.

(27) Kober, E. M.; Marshall, J. L.; Dressick, W. J.; Sullivan, B. P.; Casper, J. V.; Meyer, T. J. *Inorg. Chem.* **1985**, *24*, 2755.

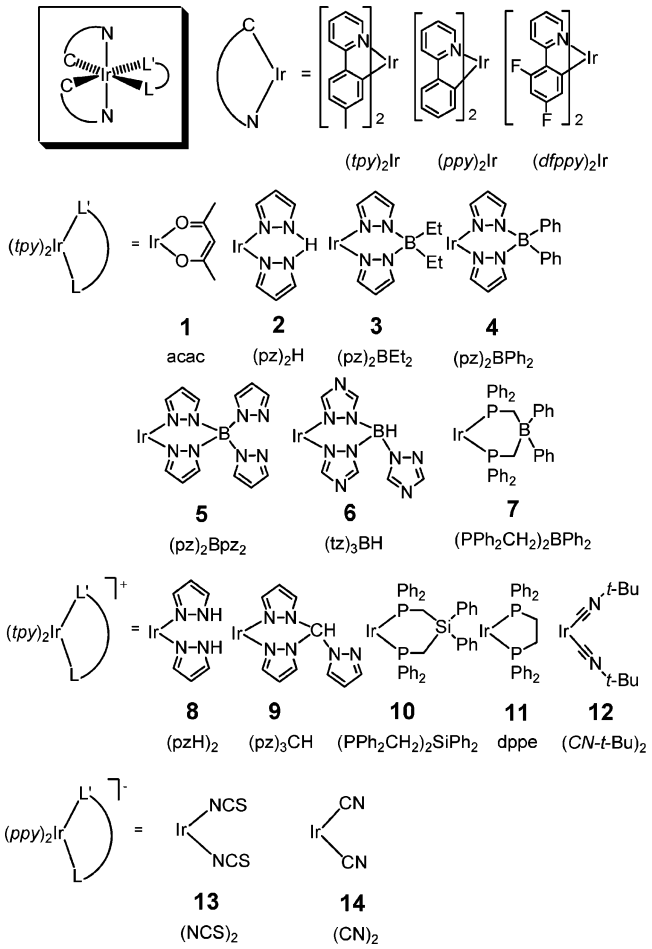

Figure 1. Structural formula and abbreviations used for the $(C\wedge N)_2$Ir(LL′) complexes.

polypyridyl complexes of Ru(II) and Os(II) has been previously explored,[27,28] a similar study has not been conducted on cyclometalated Ir(III) derivatives. The degree of metal participation in the ground and excited states of d^6 metal complexes varies greatly depending on whether the metal is from group 8 or 9, e.g., Os(II) and Ir(III), and consequently has a strong influence on the photophysical properties of the complexes.[29−31] For example, luminescence from $[Os(bpy)_3]^{2+}$ (*bpy* = 2,2′-bipyridyl) originates from a low-energy MLCT state that, despite having a high radiative rate constant ($\sim 10^5$ s^{-1}), is efficiently deactivated by metal−ligand nonradiative transitions.[32] In contrast, emission from $[Ir(bpy)_3]^{3+}$ occurs from a high-energy, ligand-centered state that is effectively quenched because of the low radiative rate for the emissive state ($\sim 10^3$ s^{-1}).[33] In addition, replacing the neutral *bpy* ligand with the formally anionic *ppy* ligand increases the electron density on the metal center, which enhances the MLCT character in the excited states of Ir complexes.[6,14,34] These differences between the metal (Os vs Ir) and ligand (*bpy* vs *ppy*) imply that systematic variation of the nonchromophoric ligand in the $(C\wedge N)_2$Ir(LL′) derivatives will be essential to generate new insights into the excited-state properties of cyclometalated Ir complexes.

The electrochemical and photophysical properties of the $(tpy)_2$Ir(LL′) complexes are discussed in detail. The lowest excited state of cyclometalated Ir complexes is identified as a dominant ligand-centered $^3\pi-\pi^*$ state with minor to significant ^{1}MLCT character.[14,21,29] The electrochemical studies of all $(tpy)_2$Ir(LL′) complexes demonstrate that the ancillary ligands increase the absorption and emission energies of $(tpy)_2$Ir(LL′) complexes by stabilizing the metal-based highest occupied molecular orbital (HOMO), leaving the lowest unoccupied molecular orbital (LUMO) largely unchanged. Besides increasing the emission energy, the lower HOMO energies increase the energy separation between the ^{1}MLCT and ^{3}LC states, which in turn modify the excited-state properties of the Ir complexes primarily by decreasing the radiative rates.

Experimental Section

The UV−visible spectra were recorded on a Hewlett-Packard 4853 diode array spectrometer. The IR spectra were obtained on a Perkin-Elmer FTIR spectrometer (model Spectrum 2000). Steady-state emission experiments at room temperature and 77 K were performed on a PTI QuantaMaster model C-60 spectrometer. Quantum efficiency measurements were carried out at room temperature in a 2-methyltetrahydrofuran (2-MeTHF) solution that was distilled over sodium. Before emission spectra were measured, the solutions were degassed by several freeze−pump−thaw cycles using a high-vacuum line equipped with a diffusion pump. Solutions of coumarin 47 (coumarin 1) in ethanol ($\Phi = 0.73$)[35] were used as a reference. The equation $\Phi_s = \Phi_r(\eta_s^2 A_r I_s/\eta_r^2 A_s I_r)$ was used to calculate the quantum yields where Φ_s is the quantum yield of the sample, Φ_r is the quantum yield of the reference, η is the refractive index of the solvent, A_s and A_r are the absorbance of the sample and the reference at the wavelength of excitation, and I_s and I_r are the integrated areas of emission bands.[36] Phosphorescence lifetime measurements were performed on an IBH Fluorocube fluorimeter by a time-correlated single photon counting method using either a 373 nm or a 403 nm LED excitation source. NMR spectra were recorded on Bruker AM 360 MHz and AMX 500 MHz instruments, and chemical shifts were referenced to residual protiated solvent. The Microanalysis Laboratory at the University of Illinois, Urbana−Champaign, performed all elemental analysis.

X-ray Crystallography. X-ray diffraction data were collected on a Bruker SMART APEX CCD diffractometer with graphite-monochromated Mo Kα radiation ($\lambda = 0.71073$ Å) at 298(2) K for $(tpy)_2Ir(PPh_2CH_2)_2BPh_2 \cdot H_2O$ and 143(2) K for $[(tpy)_2Ir(CN\text{-}t\text{-}Bu)_2](CF_3SO_3) \cdot CHCl_3$. The cell parameters for the Ir complexes were obtained from the least-squares refinement of spots (from 60 collected frames) using the SMART program. A hemisphere of the crystal data was collected up to a resolution of 0.75 Å, and the intensity data were processed using the Saint Plus program. All calculations for the structure determination were carried out using

(28) Caspar, J. V.; Meyer, T. J. *Inorg. Chem.* **1983**, *22*, 2444.
(29) Yersin, H.; Humbs, W. *Inorg. Chem.* **1999**, *38*, 5820.
(30) Zheng, K.; Wang, J.; Shen, Y.; Kuang, D.; Yun, F. *J. Phys. Chem. A* **2001**, *105*, 7248.
(31) Yersin, H.; Humbs, W.; Strasser, J. *Coord. Chem. Rev.* **1997**, *159*, 325.
(32) Kober, E. M.; Caspar, J. V.; Lumpkin, R. S.; Meyer, T. J. *J. Phys. Chem.* **1986**, *90*, 3722.
(33) Flynn, C. M., Jr.; Demas, J. N. *J. Am. Chem. Soc.* **1974**, *96*, 1959.
(34) Watts, R. J. *Comments Inorg. Chem.* **1991**, *11*, 303.
(35) Jones, G., II; Jackson, W. R.; Choi, C.-Y.; Bergmark, W. R. *J. Phys. Chem.* **1985**, *89*, 294.
(36) DePriest, J.; Zheng, G. Y.; Goswami, N.; Eichhorn, D. M.; Woods, C.; Rillema, D. P. *Inorg. Chem.* **2000**, *39*, 1955.

Table 1. Crystal Data and Summary of Intensity Data Collection and Structure Refinement for $(tpy)_2Ir(PPh_2CH_2)_2BPh_2 \cdot H_2O$ and $(tpy)_2Ir(CN\text{-}t\text{-}Bu)_2(CF_3SO_3) \cdot CHCl_3$

	$(tpy)_2Ir(PPh_2CH_2)_2BPh_2 \cdot H_2O$	$[(tpy)_2Ir(CN\text{-}t\text{-}Bu)_2](CF_3SO_3) \cdot CHCl_3$
empirical formula	$C_{62}H_{56}BIrN_2OP_2$	$C_{36}H_{39}Cl_3F_3IrN_4O_3S$
formula weight	1110.10	963.32
temperature, K	298(2)	143(2)
wavelength, Å	0.71073	0.71073
crystal system	monoclinic	monoclinic
space group	*P*2(1)/*n*	*P*2(1)/*n*
unit cell dimensions		
a (Å)	17.6248(14)	13.655(3)
b (Å)	13.6990(11)	13.262(3)
c (Å)	23.8155(19)	22.981(5)
α (deg)	90	90
β (deg)	104.034(2)	98.624(4)
γ (deg)	90	90
volume, Å^3	5578.4(8)	4114.6(15)
Z	4	4
d_{calcd}, Mg/m^3	1.365	1.555
abs coeff, mm^{-1}	2.494	3.542
F(000)	2316	1912
θ range for data collection, deg	1.30−27.50	1.63−27.47
reflns collected	32905	24489
indep reflns	12187 [*R*(int) = 0.0579]	9126 [*R*(int) = 0.0532]
refinement method	full-matrix least-squares on F^2	full-matrix least- squares on F^2
data/restraints/params	12187/0/625	9126/0/468
goodness-of-fit on F^2	0.943	1.046
final *R* indices [$I > 2\sigma(I)$]	0.0652	0.0433
R indices (all data)	0.0882	0.0588

the SHELXTL package (version 5.1).[37] Initial atomic positions were located by Patterson methods using XS, and the structure of $(tpy)_2Ir(PPh_2CH_2)_2BPh_2 \cdot H_2O$ was refined by least-squares methods using SHELX93 with 6983 independent reflections within the range of $\theta = 1.30-27.50°$ (completeness 95.2%). The data for $[(tpy)_2Ir(CN\text{-}t\text{-}Bu)_2](CF_3SO_3) \cdot CHCl_3$ were $\theta = 1.63-27.47°$ (completeness 96.7%). Absorption corrections were applied by using SADABS.[38] Calculated hydrogen positions were input and refined in a riding manner along with the attached carbons. A summary of the refinement details and resulting factors are given in Table 1.

Density Functional Theory Calculation. Density functional theory (DFT) calculations were performed using the Titan software package (Wavefunction, Inc.) at the B3LYP/LACVP** level. The HOMO and LUMO energies were determined using a minimized singlet geometry to approximate the ground state.

Electrochemistry. Cyclic voltammetry and differential pulsed voltammetry were performed using an EG&G potentiostat/galvanostat model 283. Anhydrous DMF (Aldrich) was used as the solvent under a nitrogen atmosphere, and 0.1 M tetra(*n*-butyl)-ammonium hexafluorophosphate was used as the supporting electrolyte. A silver wire was used as the *pseudo*-reference electrode, a Pt wire was used as the counter electrode, and glassy carbon was used as the working electrode. The redox potentials are based on the values measured from differential pulsed voltammetry and are reported relative to a ferrocenium/ferrocene (Fc^+/Fc) redox couple used as an internal reference (0.45 V vs saturated calomel electrode (SCE)).[39] The reversibility of reduction or oxidation was determined using cyclic voltammetry.[40] As defined, if peak anodic and peak cathodic currents have an equal magnitude under the conditions of fast scan (100 mV/s or above) and slow scan (50 mV/s), then the process is *reversible*; if the magnitudes in peak anodic and peak cathodic currents are the same in fast scan but slightly different in slow scan, the process is defined as *quasi-reversible*; otherwise, the process is defined as *irreversible*.

Synthesis. The $(tpy)_2Ir(LL')$ complexes $(tpy)_2Ir(acac)$ (**1**),[15] $(tpy)_2Ir(pz)_2H$ (**2**), $[(tpy)_2Ir(pzH)_2](CF_3SO_3)$ (**8**), $(tpy)_2Ir(pz)_2BEt_2$ (**3**), $(tpy)_2Ir(pz)_2BPh_2$ (**4**), $(tpy)_2Ir(pz)_2Bpz_2$ (**5**), $(dfppy)_2Ir(acac)$ (**1**), $(dfppy)_2Ir(pz)_2H$ (**2**), and $(dfppy)_2Ir(pz)_2Bpz_2$ (**5**) were prepared according to previous reported synthetic methods.[41] $(Bu_4N)(PPh_2CH_2)_2BPh_2$,[42] $(PPh_2CH_2)_2SiPh_2$,[42] $K(tz)_3BH$,[43] $[(tpy)_2Ir(H_2O)_2](CF_3SO_3)$,[4,41] $(Bu_4N)[(ppy)_2Ir(NCS)_2]$ (**13**) and $(Bu_4N)[(ppy)_2Ir(CN)_2]$ (**14**)[18] were prepared following published procedures. Hydrotris(pyrazolyl)methane (pz_3CH) was purchased from STREM Chemical Co. Silver trifluoromethylsulfonate (AgOTf), *tert*-butyl isocyanide (CN-*t*-Bu), bis(diphenylphosphino)ethane, and all other materials were purchased from Aldrich Chemical Co. and used without further purification.

(a) Synthesis of $(tpy)_2Ir(tz)_3BH$ (6): Iridium(III) Bis(2′-*para*-tolylpyridinato-*N*,$C^{2'}$)η^2-hydrotris(triazolyl)borate. $[(tpy)_2Ir(H_2O)_2](CF_3SO_3)$ (0.15 g, 0.2 mmol) was dissolved in 20 mL CH_3CN, and 2 equiv $K(tz)_3BH$ (0.1 g, 0.4 mmol) was added to the solution. The solution was refluxed under N_2 overnight. After cooling to room temperature, the reaction mixture was evaporated to dryness under reduced pressure. The raw product was crystallized in methanol/hexane followed by recrystallization in CH_2Cl_2/hexane. The yellow compound was obtained in a yield of 50%. ^{1}H NMR (500 MHz, $CDCl_3$), ppm: 8.20 (s, 1H), 8.04 (s, 1H), 7.81 (d, J = 8.4 Hz, 1H), 7.77 (d, J = 8.4 Hz, 1H), 7.77 (vT, J = 7.5 Hz, 1H), 7.49 (m, 3H), 7.36 (s, 1H), 7.30 (d, J = 5.6 Hz, 1H), 7.21 (s, 1H), 6.94 (vT, J = 6.6 Hz, 1H), 6.80 (d, J = 8.0 Hz, 1H), 6.77 (d, J = 8.0 Hz, 1H), 6.66 (vT, J = 6.6 Hz, 1H), 6.05 (s, 1 H), 5.98 (s, 1H), 5.2−4.2 (br, 1H), 2.09 (s, 3H), 2.05 (s, 3H). Anal. for $(tpy)_2Ir(tz_3$-

(37) Sheldrick, G. M. *SHELXTL*, version 5.1; Bruker Analytical X-ray System, Inc.: Madison, WI, 1997.
(38) Blessing, R. H. *Acta Crystallogr*. **1995**, *A51*, 33.
(39) Connelly, N. G.; Geiger, W. E. *Chem. Rev*. **1996**, *96*, 877.
(40) Harris, D. C. *Quantitative Chemical Analysis*, 6th ed.; W. H. Freeman: New York, 2003; pp 394−396.
(41) Li, J.; Djurovich, P. I.; Alleyne, B. D.; Tsyba, I.; Ho, N. N.; Bau, R.; Thompson, M. E. *Polyhedron*, **2004**, *23*, 419.
(42) (a) Thomas, J. C.; Peters, J. C. *J. Am. Chem. Soc*. **2001**, *123*, 5100. (b) Thomas, J. C.; Peters, J. C. *J. Am. Chem. Soc*. **2003**, *125*, 8870. (c) Thomas, J. C.; Peters, J. C. *Inorg. Chem*. **2003**, *42*, 5055.
(43) Shiu, K.-B.; Lee, J. Y.; Wang, Y.; Cheng, M.-C.; Wang S.-L.; Liao, F.-L. *J. Organomet. Chem*. **1993**, *453*, 211.

BH)·0.5CH_2Cl_2: found: C 46.96, H 3.31, N 19.87; calcd: C 46.54, H 3.59, N 19.57.

(b) Synthesis of [(*tpy*)$_2$Ir(pz)$_3$CH](CF$_3$SO$_3$) (9): Iridium(III) Bis(2′-*para*-tolylpyridinato-*N*,*C*$^{2′}$)[η^2-hydrotris(pyrazolyl)-methane] Trifluoromethylsulfonate. (*tpy*)$_2$Ir(H_2O)$_2$(CF_3SO_3) (0.15 g, 0.2 mmol) was dissolved in 20 mL CH_3CN, and 2 equiv pz_3CH (0.09 g, 0.4 mmol) was added to the solution. The solution was refluxed under N_2 overnight. After cooling to room temperature, the reaction mixture was evaporated to dryness under reduced pressure. The raw product was crystallized in acetone/hexane followed by recrystallization in CH_2Cl_2/hexane. The yellow-brownish compound was obtained in a yield of 35%. ^{1}H NMR (500 MHz, acetone-d_6), ppm: 8.20 (s, 1H), 8.04 (s, 1H), 7.81 (d, J = 8.4 Hz, 1H), 7.77 (d, J = 8.4 Hz, 1H), 7.77 (vT, J = 7.5 Hz, 1H), 7.49 (m, 3H), 7.36 (s, 1 H), 7.30 (d, J = 5.6 Hz, 1H), 7.21 (s, 1 H), 6.94 (vT, J = 6.6 Hz, 1H), 6.80 (d, J = 8.0 Hz, 1H), 6.77 (d, J = 8.0 Hz, 1H), 6.66 (vT, J = 6.6 Hz, 1H), 6.05 (s, 1H), 5.98 (s, 1H), 5.2−4.2 (br, 1H), 2.09 (s, 3H), 2.05 (s, 3H). Anal. for [(*tpy*)$_2$Ir-(pz_3CH)](CF_3SO_3)·0.25CH_2Cl_2: found: C 46.57, H 3.33, N 11.99; calcd: C 46.36, H 3.37, N 12.27.

(c) Synthesis of (*tpy*)$_2$Ir(PPh$_2$CH$_2$)$_2$BPh$_2$ (7): Iridium(III) Bis-(2′-*para*-tolylpyridinato-*N*,*C*$^{2′}$) Bis(diphenylphosphinomethylene)diphenylborate. [(*tpy*)$_2$Ir(H_2O)$_2$](CF_3SO_3) (0.15 g, 0.2 mmol) was dissolved in 25 mL CH_3CN, and 2 equiv (Bu_4N)[(PPh_2CH_2)$_2$-BPh_2] (0.28 g, 0.4 mmol) was added to the solution. The solution was refluxed under N_2 for 18 h. After cooling to room temperature, the reaction mixture was evaporated to dryness under reduced pressure. The yellow crystalline product (yield 50%) was obtained from column chromatography on silica using a CH_2Cl_2 mobile phase. ^{1}H NMR (500 MHz, $CDCl_3$), ppm: 8.72 (d, J = 2.8 Hz, 2H), 7.48−7.39 (m, 6H), 7.20 (dd, J = 8.0, 8.0 Hz, 4H), 7.12 (d, J = 4.2 Hz, 2H), 7.09−6.94 (m, 10H), 6.80−6.70 (m, 8H), 6.56 (d, J = 3.8 Hz, 2H), 6.45 (dd, J = 7.5, 7.5 Hz, 4H), 6.30 (dd, J = 7.0, 7.0 Hz, 4H), 6.15 (s, 2H), 2.30 (m, 2H), 2.21 (m, 2H), 2.05 (s, 6H). Anal. for (*tpy*)$_2$Ir[(PPh_2CH_2)$_2$$BPh_2$]: found: C 68.07, H 4.80, N 2.70; calcd: C 68.19, H 4.98, N 2.57.

(d) Synthesis of [(*tpy*)$_2$Ir(PPh$_2$CH$_2$)$_2$SiPh$_2$](CF$_3$SO$_3$) (10): Iridium(III) Bis(2′-*para*-tolylpyridinato-*N*,*C*$^{2′}$)[bis-(diphenylphosphinomethylene)diphenylsilane] Trifluoromethylsulfonate. [(*tpy*)$_2$Ir(H_2O)$_2$](CF_3SO_3) (0.15 g, 0.2 mmol) was dissolved in 25 mL CH_2Cl_2, and 2 equiv $Ph_2Si(CH_2PPh_2)_2$ (0.23 g, 0.4 mmol) was added to the solution. The solution was stirred at room temperature overnight and was evaporated to dryness under reduced pressure. The yellow product (yield 60%) was obtained by recrystallization in CH_2Cl_2/hexane. ^{1}H NMR (500 MHz, $CDCl_3$), ppm: 8.59 (d, J = 5.8 Hz, 2H), 7.73 (dd, J = 8.4, 8.4 Hz, 2H), 7.47 (m, 6H), 7.39 (dd, J = 7.0, 7.0 Hz, 4H), 7.36−7.26 (m, 8H), 6.98 (m, 8H), 6.91 (dd, J = 7.0, 7.0 Hz, 2H), 6.62 (dd, J = 7.8, 7.8 Hz, 6H), 6.21 (d, J = 8.4, Hz, 4H), 5.98 (s, 2H), 2.62−2.46 (m, 4H), 2.04 (s, 6H). Anal. for (*tpy*)$_2$Ir[(PPh_2CH_2)$_2$$SiPh_2$]($CF_3$-$SO_3$)·0.5$CH_2Cl_2$: found: C 58.96, H 4.24, N 2.30; calcd: C 58.63, H 4.26, N 2.15.

(e) Synthesis of [(*tpy*)$_2$Ir(dppe)](CF$_3$SO$_3$) (11): Iridium(III) Bis(2′-*para*-tolylpyridinato-*N*,*C*$^{2′}$)[bis(diphenylphosphino)-ethane] Trifluoromethylsulfonate. [(*tpy*)$_2$Ir(H_2O)$_2$](CF_3SO_3) (0.15 g, 0.2 mmol) was dissolved in 25 mL dicholoroethane, and 2 equiv bis(diphenylphosphino)ethane (0.16 g, 0.4 mmol) was added to the solution. The solution was refluxed under N_2 overnight and was evaporated to dryness under reduced pressure. The raw product was crystallized in CH_2Cl_2/hexane followed by recrystallization in CH_2Cl_2/ether. The yellowish compound was obtained in a yield of 30%. ^{1}H NMR (500 MHz, acetone-d_6), ppm: 7.90 (d, J = 5.7 Hz, 2H), 7.84 (vT, J = 8.0 Hz, 6H), 7.72 (d, J = 8.0 Hz, 2H), 7.62 (vT, J = 8.0 Hz, 2H), 7.47 (vT, J = 7.5 Hz, 2H), 7.37 (vT, J = 7.5 Hz, 4H), 7.06 (vT, J = 7.0 Hz, 2H), 6.96−6.87 (m, 6H), 6.78 (vT, J = 8.9 Hz, 4H), 6.44 (vT, J = 7.1 Hz, 2H), 6.22 (s, 2H), 4.12−3.93 (m, 2H), 3.06 (d, J = 9.0 Hz, 2H), 2.10 (s, 6H). Anal. for [(*tpy*)$_2$Ir(dppe)](CF_3SO_3)·H_2O: found: C 55.23, H 4.01, N 2.07; calcd: C 55.98, H 4.24, N 2.56.

(f) Synthesis of [(*tpy*)$_2$Ir(CN-t-Bu)$_2$](CF$_3$SO$_3$) (12): Iridium-(III) Bis(2′-*para*-tolylpyridinato-*N*,*C*$^{2′}$) Bis(*tert*-butyl isocyanide) Trifluoromethylsulfonate. [(*tpy*)$_2$Ir(H_2O)$_2$](CF_3SO_3) (0.15 g, 0.2 mmol) and 0.2 g *t*-BuNC were added to 20 mL of CH_2Cl_2. The solution was stirred for 2 days at room temperature. The reaction mixture was evaporated to dryness under reduced pressure, and the yellow product (yield 35%) was obtained by successive recrystallization in CH_2Cl_2/hexane. ^{1}H NMR (500 MHz, $CDCl_3$), ppm: 8.93 (d, J = 5.6 Hz, 2H), 7.97 (dd, J = 8.0, 8.0 Hz, 2H), 7.90 (d, J = 8.0 Hz, 2H), 7.50 (d, J = 8.0 Hz, 2H), 7.41 (vT, J = 6.4 Hz, 2H), 6.77 (d, J = 7.6 Hz, 2H), 6.05 (s, 1H), 5.91 (s, 2H), 2.04 (s, 6H), 1.31 (s, 18H). IR: 2192, 2168 cm^{-1} (terminal C≡N stretch). Anal. for [(*tpy*)$_2$Ir(CN-*t*-Bu)$_2$](CF_3SO_3): found: C 48.96, H 4.38, N 6.48; calcd: C 49.81, H 4.54, N 6.64.

(g) Synthesis of (*dfppy*)$_2$Ir(PPh$_2$CH$_2$)$_2$BPh$_2$ (7): Iridium(III) Bis(4′,6′-difluorophenylpyridinato-*N*,*C*$^{2′}$) Bis(diphenylphosphinomethylene)diphenylborate. This yellow compound was prepared analogous to the synthesis of (*tpy*)$_2$Ir[$Ph_2B(CH_2PPh_2)_2$] and was obtained after chromatography on a silica/CH_2Cl_2 column in 55% yield. ^{1}H NMR (500 MHz, $CDCl_3$), ppm: 8.84 (d, J = 2.8 Hz, 2H), 7.61 (dd, J = 4.2, 3.8 Hz, 2H), 7.53 (dd, J = 8.0, 8.0 Hz, 2H), 7.42 (d, J = 3.8 Hz, 4H), 7.18−7.04 (m, 10H), 6.99 (dd, J = 7.0, 7.0 Hz, 2H), 6.90−6.76 (m, 8H), 6.65 (dd, J = 7.5, 7.5 Hz, 4H), 6.40−6.26 (m, 6H), 5.84 (m, 2H), 2.29 (m, 2H), 2.21 (m, 2H). Anal. for (*dfppy*)$_2$Ir[(PPh_2CH_2)$_2$$BPh_2$]: found: C 62.75, H 3.92, N 2.68; calcd: C 63.44, H 4.08, N 2.47.

(h) Synthesis of [(*dfppy*)$_2$Ir(CN-*t*-Bu)$_2$](CF$_3$SO$_3$) (12): Iridium-(III) Bis(4′,6′-difluorophenylpyridinato-*N*,*C*$^{2′}$)bis(*tert*-butyl isocyanide) Trifluoromethylsulfate. This yellow compound was prepared analogous to the synthesis of (*tpy*)$_2$Ir(CN-*t*-Bu)$_2$(CF_3SO_3) and was obtained by further recrystallization in CH_2Cl_2/hexane twice in 40% yield. ^{1}H NMR (360 MHz, $CDCl_3$), ppm: 9.05 (d, J = 5.9 Hz, 2H), 8.35 (d, J = 8.3 Hz, 2H), 8.03 (vT, J = 7.3 Hz, 2H), 7.52 (vT, J = 7.3 Hz, 2H), 6.49 (m, 2H), 5.55 (dd, J = 7.8, 2.4 Hz, 2H), 1.39 (s, 18H). IR: 2204, 2183 cm^{-1} (terminal C≡N stretch). Anal. for (*dfppy*)$_2$Ir(CN-*t*-Bu)$_2$(CF_3SO_3): found: C 44.17, H 3.18, N 6.01; calcd: C 44.64, H 3.41, N 6.31.

Results and Discussion

Synthesis and Characterization. The (*tpy*)$_2$Ir(LL′) complexes in Figure 1 were prepared from the chloride-bridged Ir(III) dimer, [(*tpy*)$_2$Ir(μ-Cl)]$_2$, using three different routes. The *tpy*, as opposed to the parent 2-phenylpyridyl (*ppy*), ligand was chosen in order to increase solubility, and thereby ease synthesis, and also to simplify characterization by NMR spectroscopy and X-ray crystallography. Only minor perturbation is caused by the methyl substituent in the photophysical properties of the (*tpy*)$_2$Ir(LL′) complexes relative to the *ppy* analogues.[15] We have previously shown that the Ir dimer can be readily converted to emissive, monomeric complex by treating the dimer with acetylacetone and base (eq 1).[15] Likewise, the synthesis and characterization of (*tpy*)$_2$Ir(LL*) (LL* = pyrazolyl or pyrazolyl borate) complexes have been discussed in an earlier report.[41] Reaction of the dichloro-bridged dimer with excess bis(pyrazolyl)-

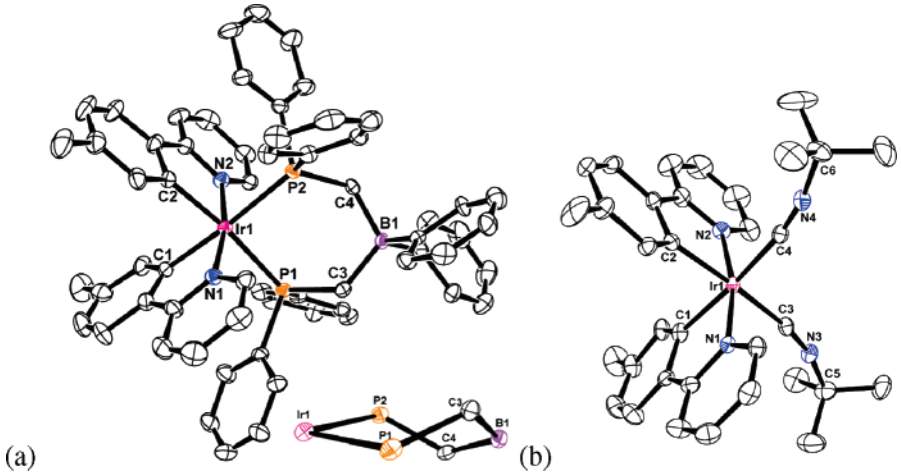

Figure 2. ORTEP drawings of (a) $(tpy)_2Ir(PPh_2CH_2)_2BPh_2 \cdot H_2O$ (the Ir-P-C-B-C-P ring is shown in the inset) and (b) $(tpy)_2Ir(CN\text{-}t\text{-}Bu)_2(CF_3SO_3) \cdot CHCl_3$. The thermal ellipsoids for the image represent 25% probability limit. The hydrogen atoms, counteranion, and solvent are omitted for clarity.

Table 2. Selected Bond Distances (Å) for $(tpy)_2Ir(acac)$, $(tpy)_2Ir(pz)_2H$, $[(tpy)_2Ir(pzH)_2](CF_3SO_3)$, $(tpy)_2Ir(pz)_2BEt_2$, $(tpy)_2Ir(pz)_2Bpz_2$, $(tpy)_2Ir(PPh_2CH_2)BPh_2$, and $(tpy)_2Ir(CN\text{-}t\text{-}Bu)_2(CF_3SO_3)$

$(tpy)_2Ir(X_1X_2)$	Ir−C_1	Ir−C_2	Ir−N_1	Ir−N_2	Ir−X_1	Ir−X_2
1 $(tpy)_2Ir(acac)$	1.982(6)	1.985(7)	2.023(5)	2.040(5)	2.161(4)	2.136(4)
2 $(tpy)_2Ir(pz)_2H$	2.005(12)	2.020(13)	2.031(10)	2.042(9)	2.155(9)	2.181(10)
8 $[(tpy)_2Ir(pzH)_2](CF_3SO_3)$	1.995(12)	1.995(12)	2.045(10)	2.045(10)	2.180(9)	2.180(10)
3 $(tpy)_2Ir(pz)_2BEt_2$	2.005(4)	2.007(4)	2.030(3)	2.033(3)	2.141(3)	2.137(3)
5 $(tpy)_2Ir(pz)_2Bpz_2$	2.009(5)	2.007(5)	2.044(4)	2.039(4)	2.147(4)	2.137(4)
7 $(tpy)_2Ir(PPh_2CH_2)_2BPh_2$	2.047(9)	2.057(9)	2.082(7)	2.083(7)	2.420(2)	2.431(2)
11 $[(tpy)_2Ir(CN\text{-}t\text{-}Bu)_2](CF_3SO_3)$	2.072(5)	2.047(5)	2.059(4)	2.061(4)	2.004(6)	2.018(6)

borate ligand leads only to formation of a protonated-dipyrazolyl Ir complex, $(tpy)_2Ir(pz)_2H$ (eq 2).[41] Therefore, the chloride-free Ir complex, $[(tpy)_2Ir(H_2O)_2](CF_3SO_3)$, was prepared by chloride abstraction with CF_3SO_3Ag and used in the syntheses of Ir complexes with bis(pyrazolyl)borate ligands, e.g., $(tpy)_2Ir(pz)_2Bpz_2$ (eq 3). Similarly, $[(tpy)_2Ir(H_2O)_2](CF_3SO_3)$ readily reacts with the anionic ligands of bidentate borates, e.g., $(tz)_3BH^-$, and $(PPh_2CH_2)_2BPh_2^-$, and their neutral analogues to form the corresponding $(tpy)_2Ir(LL')$ complexes.

$$[(tpy)_2Ir(\mu\text{-}Cl)]_2 + \text{excess acacH} \xrightarrow[C_2H_4Cl_2,\ \text{reflux}]{Na_2CO_3} (tpy)_2Ir(acac) \quad (1)$$

$$[(tpy)_2Ir(\mu\text{-}Cl)]_2 + \text{excess } KBpz_4 \xrightarrow[\text{reflux}]{CH_3CN} (tpy)_2Ir(pz)_2H \quad (2)$$

$$[(tpy)_2Ir(\mu\text{-}Cl)]_2 \xrightarrow[CH_2Cl_2/MeOH]{AgOTf} [(tpy)_2Ir(H_2O)_2](CF_3SO_3) \xrightarrow[CH_3CN,\ \text{reflux}]{\text{excess } KBpz_4} (tpy)_2Ir(pz)_2Bpz_2 \quad (3)$$

Single crystals of $(tpy)_2Ir[(PPh_2CH_2)_2BPh_2] \cdot H_2O$ were prepared by slow evaporation of a chloroform solution, while single crystals of $[(tpy)_2Ir(CN\text{-}t\text{-}Bu)_2](CF_3SO_3) \cdot CHCl_3$ were grown from chloroform/hexane. Molecular plots of $(tpy)_2Ir[(PPh_2CH_2)_2BPh_2]$ and $(tpy)_2Ir(CN\text{-}t\text{-}Bu)_2^+$ are shown in Figure 2; crystallographic data are given in Table 1. The Ir-P-C-B-C-P ring of $(tpy)_2Ir[(PPh_2CH_2)_2BPh_2]$ adopts a twisted-boat conformation (Figure 2a, inset) similar in structure to that reported in other complexes of the same ligand, e.g., $[Me_2Pt(PPh_2CH_2)_2BPh_2][ASN]$ (ASN = 5-azonia-spiro[4.4]nonane)),[42a,b] or in the Li salt, $[(PPh_2CH_2)_2BPh_2][Li(TMEDA)_2]$ (TMEDA = *N*,*N*′,*N*′-tetramethylethylene-1,2-diamine).[42c] The CN-*t*-Bu ligands in $(tpy)_2Ir(CN\text{-}t\text{-}Bu)_2^+$ are slightly distorted (average Ir−C−N = 170°, average C−N−C = 167°). Similar deviations from linearity have been reported for the CN-*t*-Bu ligands in other Rh or Ir complexes such as $[(\eta^2\text{-acac})_2Rh(\mu\text{-}CPh_2)_2Rh(CN\text{-}t\text{-}Bu)_2]$,[44] $[(t\text{-}BuNC)_2(Cl)Ir(\mu\text{-pz})_2Ir(\eta^1\text{-}CH_2Ph)(CN\text{-}t\text{-}Bu)_2]$,[45] and $[Cp^*Ir(CN\text{-}t\text{-}Bu)(\mu\text{-}S)_2Ir(CN\text{-}t\text{-}Bu)Cp^*]$.[46]

Selected bond lengths for seven Ir complexes with the same "tpy_2Ir" fragment, including previously reported $(tpy)_2Ir(acac)$,[15] $(tpy)_2Ir(pz)_2H$,[41] $[(tpy)_2Ir(pzH)_2](CF_3SO_3)$,[41] $(tpy)_2Ir(pz)_2Bpz_2$,[41] and $(tpy)_2Ir(pz)_2BEt_2$,[41] are provided in Table 2. All of these complexes have an octahedral coordination geometry around Ir, retaining the *cis*-C,C *trans*-N,N chelate disposition of the chloride-bridged precursor complex, $[(tpy)_2Ir(\mu\text{-}Cl)]_2$. The N−Ir−N angles for the two *trans*-N,N atoms in these complexes are between 169 and 175°. The Ir−C_{aryl} bond lengths of $(tpy)_2Ir(PPh_2CH_2)_2BPh_2$ (2.047(9), 2.057(9) Å) and $[(tpy)_2Ir(CN\text{-}t\text{-}Bu)_2]^+$ (2.047(5), 2.072(5) Å) are longer than their counterparts in $(tpy)_2Ir(acac)$ (1.982(6), 1.985(7) Å). However, the Ir−C_{aryl} bond lengths of the $(tpy)_2Ir(LL')$[41] complexes with pyrazolyl ligands (range = 1.995(12) −2.020(13) Å) are not significantly different than those found in $(tpy)_2Ir(acac)$.

(44) Herber, U.; Pechmann, T.; Weberndorfer, B.; Ilg, K.; Werner, H. *Chem.—Eur. J.* **2002**, *8* (1), 309.
(45) (a) Tejel, C.; Ciriano, M. A.; Lopez, J. A.; Lahoz, F. J.; Oro, L. A. *Organometallics* **1998**, *17*, 1449. (b) Tejel, C.; Ciriano, M. A.; Lopez, J. A.; Lahoz, F. J.; Oro, L. A. *Organometallics* **2000**, *19*, 4977.
(46) Dobbs, D. A.; Bergman, R. G. *Inorg. Chem.* **1994**, *33*, 5329.

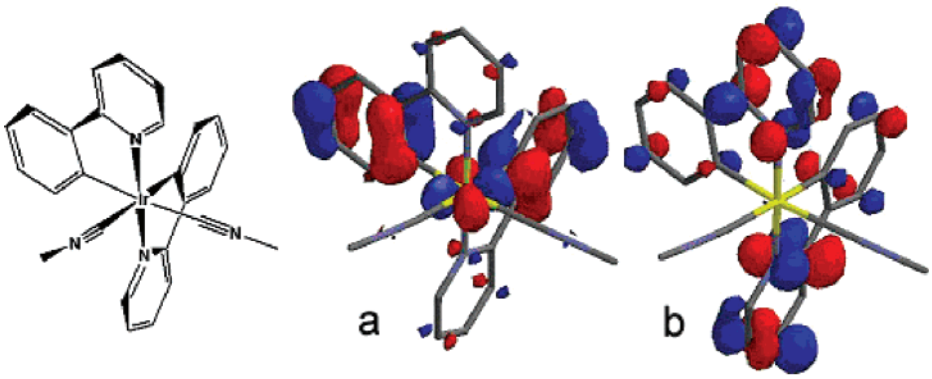

Figure 3. The HOMO (a) and LUMO (b) surface of $(ppy)_2Ir(CN\text{-}Me)_2^+$ from DFT calculations. The HOMO orbital consists mainly of a mixture of phenyl-π and Ir-d orbitals, while the LUMO orbital is largely localized on the pyridyl moiety.

Table 3. Redox Properties of $(tpy)_2Ir(LL')$ Complexes[e]

$(C\wedge N)_2Ir(LL')$	$E_{1/2}^{Ox}$ (V)	$E_{1/2}^{Red}$ (V)	$\Delta E_{1/2}$ (V)	$E_{1_{MLCT}}$ (V)
1 $(tpy)_2Ir(acac)$	0.41	−2.68	3.09	3.02
2 $(tpy)_2Ir(pz)_2H$	0.55,[d] 0.77[d]	−2.65[d]	3.20	3.16
3 $(tpy)_2Ir(pz)_2BEt_2$	0.63,[d] 0.77[d]	−2.66[c]	3.29	3.18
4 $(tpy)_2Ir(pz)_2BPh_2$	0.67[d]	−2.64	3.31	3.17
5 $(tpy)_2Ir(pz)_2Bpz_2$	0.72[d]	−2.64	3.36	3.24
6 $(tpy)_2Ir(tz)_3BH$	0.82[a]	−2.56	3.38	3.25
7 $(tpy)_2Ir(PPh_2CH_2)_2BPh_2$	0.81[a,d]	−2.62	3.43	3.35
8 $[(tpy)_2Ir(pzH)_2]CF_3SO_3)$	0.75[a]	−2.40[d]	3.15	3.27
9 $[(tpy)_2Ir(pz)_3CH](CF_3SO_3)$	0.89[a]	−2.43[d]	3.32	3.29
10 $[(tpy)_2Ir(PPh_2CH_2)_2SiPh_2](CF_3SO_3)$	1.10[d]	−2.42[c]	3.52	3.44
11 $[(tpy)_2Ir(dppe)](CF_3SO_3)$	1.03[b,d]	−2.46	3.49	3.46
12 $[(tpy)_2Ir(CN\text{-}t\text{-}Bu)_2](CF_3SO_3)$	1.23[b,d]	−2.39[d]	3.62	3.56
13 $(NBu_4)[(ppy)_2Ir(NCS)_2]$	0.42[d]	−2.71[d]	3.13	3.12
14 $(NBu_4)[(ppy)_2Ir(CN)_2]$	0.50[d]	−2.78	3.28	3.25

[e] Redox measurements were carried out in DMF solution unless noted: (a) in CH_2Cl_2; (b) in CH_3CN. The redox values are reported relative to Fc^+/Fc. The electrochemical process is reversible unless noted: (c) quasi-reversible; (d) irreversible.

DFT Calculations. B3LYP/LACVP** DFT calculations were carried out on the $[(ppy)_2Ir(CN\text{-}Me)_2]^+$ complex to ascertain the influence of isocyanide ligands on the bis-cyclometalated Ir complexes. A similar theoretical approach has been used to investigate the ground- and excited-state properties of related cyclometalated Ir and Pt compounds.[16,19,47] The calculated metric parameters of $[(ppy)_2Ir(CN\text{-}Me)_2]^+$ ($Ir-C_{aryl}$ (2.08 Å), Ir−N (2.10 Å), $Ir-C_{CN-Me}$ (2.04 Å)) are similar to the values found in $[(tpy)_2Ir(CN\text{-}t\text{-}Bu)_2]^+$ (Table 2). The calculated singlet state energy[48] of $[(ppy)_2Ir(CN\text{-}Me)_2]^+$ is 4.24 eV. The HOMO and LUMO surfaces for $[(ppy)_2Ir(CN\text{-}Me)_2]^+$ are illustrated in Figure 3. The orbital contours correspond quite closely to the HOMO and LUMO surfaces reported for $(ppy)_2Ir(acac)$.[47] The HOMO consists principally of a mixture of phenyl-π and Ir-d orbitals, whereas the LUMO is localized largely on the *ppy* orbitals with very little metal orbital character. Interestingly, the two ancillary ligands appear to contribute very little electron density to either the HOMO or LUMO. The HOMO surfaces for the complex suggest a possible overlap between the metal-phenyl and isocyanide orbitals. However, no such clear interaction exists between the *ppy* and isocyanide orbitals because the LUMO is predominantly distributed on the pyridyl-π orbitals, which are orthogonal to the isocyanide orbitals. Thus, the isocyanides can only directly interact with the cyclometalating ligands in the HOMO via the metal orbitals, and consequently this leaves the LUMO energy largely unperturbed, as confirmed by electrochemical analysis (vide infra). This electronic model, where the ancillary ligand interacts strongly only with the HOMO, is believed to apply to all the other $(tpy)_2Ir(LL')$ complexes as well.

Electrochemistry. The electrochemical properties of the $(tpy)_2Ir(LL')$ complexes, as well as for $(Bu_4N)[(ppy)_2Ir(NCS)_2]$ (**13**) and $(Bu_4N)[(ppy)_2Ir(CN)_2]$ (**14**),[49] were examined using cyclic voltammetry, and the values of redox potentials were determined using differential pulsed voltammetry (Table 3). All of the electrochemical data reported here were measured relative to an internal ferrocenium/ferrocene reference (Fc^+/Fc). The electrochemistry of related tris cyclometalated Ir(III) complexes, e.g., *fac*-$Ir(ppy)_3$, has been thoroughly studied.[16,50] Oxidation is considered to be a metal-aryl centered process, whereas reduction is localized mainly on the pyridyl rings of the cyclometalating ligands.[50] Thus, if no other competitive oxidation or reduction process occurs in the ancillary ligand, each $(tpy)_2Ir(LL')$ complex should only display a single one-electron oxidation (occurring at the $(tpy)_2Ir$-based HOMO) and two one-electron reductions

(47) Hay, P. J. *J. Phys. Chem. A* **2002**, *106*, 1634.
(48) The singlet state energy is estimated from the difference between the calculated HOMO and LUMO energies.
(49) The redox potentials we measure for compounds **13** and **14** are considerably different from those reported in ref 18. In particular, the reduction potentials we observe in DMF lie outside the range of accessible potentials for the CH_2Cl_2 solvent (used in ref 18).
(50) Ohsawa, Y.; Sprouse, S.; King, K. A.; DeArmond, M. K.; Hanck, K. W.; Watts, R. J. *J. Phys. Chem.* **1987**, *91*, 1047.

Table 4. Photophysical Properties of $(tpy)_2Ir(LL')$ Complexes[a]

		emission at RT					emission at 77 K	
$(C\wedge N)_2Ir(LL')$	abs, λ_{max} λ(nm) $\{\epsilon, 10^3\ cm^{-1}\ M^{-1}\}$	λ_{max} (nm)	τ (μs)	Φ_{PL}	k_r $10^5\ s^{-1}$	k_{nr} $10^5\ s^{-1}$	λ_{max} (nm)	τ (μs)
1 $(tpy)_2Ir(acac)$	269 (40.5), 406 (4.1), 451 (2.8), 488 (1.0)	512	1.4	0.38	2.7	4.4	500	3.8
2 $(tpy)_2Ir(pz)_2H$	268 (37.1), 392 (4.8), 478 (0.42)	490	2.2	0.44	2.0	2.6	480	4.2
8 $[(tpy)_2Ir(pzH)_2](CF_3SO_3)$	267 (40.0), 382 (4.5), 472 (0.17)	490	2.4	0.26	1.1	3.1	480	3.7
3 $(tpy)_2Ir(pz)_2BEt_2$	266 (36.0), 390 (5.1), 477 (0.35)	484	2.6	0.52	2.0	1.8	480	3.3
4 $(tpy)_2Ir(pz)_2BPh_2$	266 (40.0), 391 (4.8), 475 (0.31)	484	3.4	0.49	1.4	1.5	474	4.1
5 $(tpy)_2Ir(pz)_2Bpz_2$	263 (40.0), 383 (5.1), 472 (0.25)	480	3.5	0.52	1.5	1.4	473	4.2
6 $(tpy)_2Ir(tz)_3BH$	259 (38.0), 382 (4.5), 471 (0.16)	478	4.1	0.55	1.3	1.1	470	5.1
9 $[(tpy)_2Ir(pz)_3CH](CF_3SO_3)$	258 (40.2), 377 (4.9), 469 (0.16)	476	3.0	0.33	1.1	2.2	469	4.2
7 $(tpy)_2Ir(PPh_2CH_2)_2BPh_2$	250 (41.5), 370 (4.5), 463 (0.04)	468	4.7	0.038	0.08	2.0	462	23.5
10 $[(tpy)_2Ir(PPh_2CH_2)_2SiPh_2]$ (CF_3SO_3)	260 (39.0), 322 (14.0), 360 (7.4), 464 (0.04)	468	1.1	0.006	0.05	9.0	462	26.2
11 $[(tpy)_2Ir(dppe)](CF_3SO_3)$	250 (34.3), 267 (26.3), 322 (8.6), 358 (5.7), 425 (0.06), 456(0.03)	458	2.1	0.005	0.03	4.7	452	32.3
12 $[(tpy)_2Ir(CN\text{-}t\text{-}Bu)_2]$ (CF_3SO_3)	260 (33.5), 315 (15.8), 348 (12.1), 422 (0.07), 452 (0.03)	458	35.6	0.28	0.08	0.20	454	45.4
13 $(NBu_4)[(ppy)_2Ir(NCS)_2]$	263 (42.3), 336 (7.4), 398 (3.8), 444 (2.3), 482 (0.59)	508	1.5	0.40	2.7	4.0	486	3.0
14 $(NBu_4)[(ppy)_2Ir(CN)_2]$	258 (36.3), 344 (6.0.9), 381 (4.9), 462 (0.25)	476	2.6	0.48	1.8	2.0	458	4.8

[a] The absorption spectra were measured in CH_2Cl_2, and the emission spectra were measured in 2-MeTHF solution.

(occurring at each pyridyl ring of the *tpy* ligands). Under the current experimental conditions, i.e., anhydrous and nitrogen-purged DMF solution, one reduction is clearly observed for all $(tpy)_2Ir(LL')$ complexes. The ancillary ligands themselves are difficult to reduce, so the first reduction process can be assigned to one of the pyridyl rings of the "$(tpy)_2Ir$" fragment.[47,50] The reduction potentials of the neutral $(tpy)_2Ir(LL')$ complexes stay in a narrow range (-2.56 to -2.68 V), which indicates that the LUMO is little affected by the nature of the LL′ ligand.

Contrary to the relatively invariant reduction potentials of neutral $(tpy)_2Ir(LL')$ complexes, the corresponding oxidation potentials span a wider range (0.41−0.82 V). Increasing the ligand field strength of the ancillary ligands leads to higher oxidation potentials for the $(tpy)_2Ir(LL')$ complexes. For example, $(tpy)_2Ir(pz)_2Bpz_2$ has the highest oxidation potential among all neutral $(tpy)_2Ir(LL^*)$ (LL* = pyrazolyl ligands) complexes due to the relatively high ligand field strength of Bpz_4^-.[51] Coordination of stronger π-acid ancillary ligands, e.g., diphosphines, onto the $(tpy)_2Ir(LL')$ complexes leads to further increases in the oxidation potential. Although the DFT calculations suggest that the ancillary ligands do not contribute significant electron density to the HOMO of the $(tpy)_2Ir(LL')$ compounds, they still can influence the HOMO energy by interacting with the Ir d-orbitals. Thus, ancillary ligands with stronger ligand field strength stabilize the HOMO. In addition, the $(tpy)_2Ir(pz)_2BEt_2$ and $(tpy)_2Ir(pz)_2H$ complexes display a second oxidation process that can be ascribed to oxidation processes involving the ancillary ligands. For $(tpy)_2Ir(pz)_2BEt_2$, the electron-rich boron atom and comparably weak B−C bonds may be sites of oxidation,[52] as evidenced by the fact that $Na(pz)_2BEt_2$ has an irreversible oxidation (ca. 0.4 V vs Fc^+/Fc) in a dichloroethane solution. For $(tpy)_2Ir(pz)_2H$, on the other hand, the acidic proton in the "$(pz)_2H$" ligand can undergo solvent-induced deprotonation in the oxidized complex to generate additional electroactive species.[53]

The redox potentials of cationic $(tpy)_2Ir(LL')$ complexes are shifted by roughly 200−300 mV to more positive values relative to potentials found in the neutral analogues. The anodic shifts are due to the overall positive charge of the complexes. Regardless, the redox potentials display trends similar to those observed in the neutral complexes; the reduction potentials for cationic complexes fall in a narrow range (-2.39 to -2.43 V), whereas the oxidation potentials vary more widely (0.75−1.23 V).

Electronic Spectroscopy. The room-temperature (RT) absorption and emission spectra and low-temperature (77 K) spectra were recorded for all $(tpy)_2Ir(LL')$ complexes (Table 4). A typical example of absorption and emission spectra at RT displayed by the $(tpy)_2Ir(LL')$ complexes is shown in Figure 4 for $(tpy)_2Ir(pz)_2Bpz_2$. Three characteristic types of well-resolved absorption bands are observed. High-energy, intense absorption bands (250−270 nm, $\epsilon \approx 4.0 \times 10^4\ cm^{-1}\ M^{-1}$) can be assigned to allowed $^1(\pi-\pi^*)$ transitions of the *tpy* ligand.[15,54−56] The energies and extinction coefficients of these bands correlate well with similar absorption features observed in 2′-*para*-tolylpyridine (*tpy*H). Weaker bands located at longer wavelength (350−440 nm, $\epsilon = 1000-8000\ cm^{-1}\ M^{-1}$) can be assigned to Ir → *tpy* charge-transfer transitions.[15,18] The energies of these MLCT transitions are only weakly solvatochromic, undergoing a 6 nm red-shift in nonpolar (hexanes) solvent, indicating a ground state that is more polar than the excited state. The weak, lowest energy

(51) Sohrin, Y.; Kokusen, H.; Matsui, M. *Inorg. Chem.* **1995**, *34*, 3928.
(52) Pal, P. K.; Chowdhury, S.; Drew, M. G. B.; Datta, D. *New J. Chem.* **2002**, *26*, 367.
(53) Haga, M. *Inorg. Chim. Acta* **1983**, *75*, 29.
(54) Garces, F. O.; King, K. A.; Watts, R. J. *Inorg. Chem.* **1988**, *27*, 3464.
(55) Colombo, M. G.; Brunold, T. C.; Riedener, T.; Güdel, H. U.; Förtsch, M.; Bürgi, H.-B. *Inorg. Chem.* **1994**, *33*, 545.
(56) Carlson, G. A.; Djurovich, P. I.; Watts, R. J. *Inorg. Chem.* **1993**, *32*, 4483.

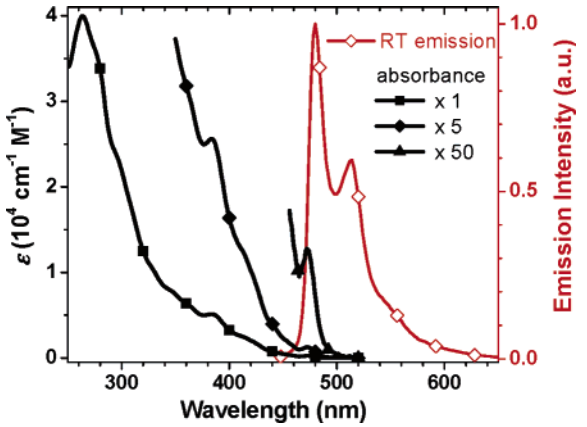

Figure 4. Room-temperature absorption and emission spectra of $(tpy)_2$Ir-$(pz)_2Bpz_2$. The absorption spectrum (filled symbols) was measured in CH_2Cl_2, and the emission spectrum (empty symbols) was measured in 2-methyltetrahydrofuran (2-MeTHF).

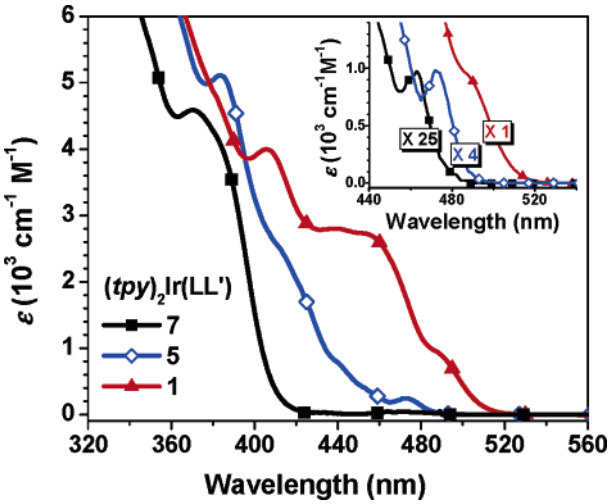

Figure 5. ^{1}MLCT absorption spectra of $(tpy)_2Ir(PPh_2CH_2)_2BPh_2$ (**7**), $(tpy)_2$-$Ir(pz)_2Bpz_2$ (**5**), and $(tpy)_2Ir(acac)$ (**1**) complexes in CH_2Cl_2. The T_1 absorption transitions are shown in the inset.

absorption band (472 nm, $\epsilon = 250$ cm^{-1} M^{-1}) can be identified as a triplet transition (T_1) on the basis of the small energy shift (350 cm^{-1}) between absorption and emission at room temperature.

A comparison of lowest energy absorption features among $(tpy)_2Ir(acac)$, $(tpy)_2Ir(pz)_2Bpz_2$, and $(tpy)_2Ir(PPh_2CH_2)_2BPh_2$ is shown in Figure 5. For $(tpy)_2Ir(acac)$, a series of strong overlapping absorption bands diminish in energy down to 500 nm. The absorption bands between 420 and 500 nm can be assigned to a combination of singlet and triplet MLCT transitions involving both the *tpy* and acac ligands on the basis of time-dependent DFT calculations of the $(ppy)_2Ir$ analogue.[47] The peak at 406 nm (3.06 eV) coincides in energy with the difference in electrochemical oxidation and reduction potentials (3.09 V) and can therefore be assigned to a ^{1}MLCT transition between the HOMO and LUMO. For both $(tpy)_2Ir(pz)_2Bpz_2$ and $(tpy)_2Ir(PPh_2CH_2)_2BPh_2$ complexes, the intensities of the mixed singlet and triplet MLCT transitions at wavelengths greater than 420 nm are markedly attenuated, whereas strong ^{1}MLCT transitions still occur between 350 and 410 nm. The ^{1}MLCT and T_1 transition energies increase with change in the ancillary ligand ($acac^-$ < Bpz_4^- < $(PPh_2CH_2)_2BPh_2^-$). However, while the ^{1}MLCT energies increase with only minor changes in intensity, the increase in the T_1 absorption energy coincides with a pronounced decrease in the extinction coefficient (Figure 5, inset).

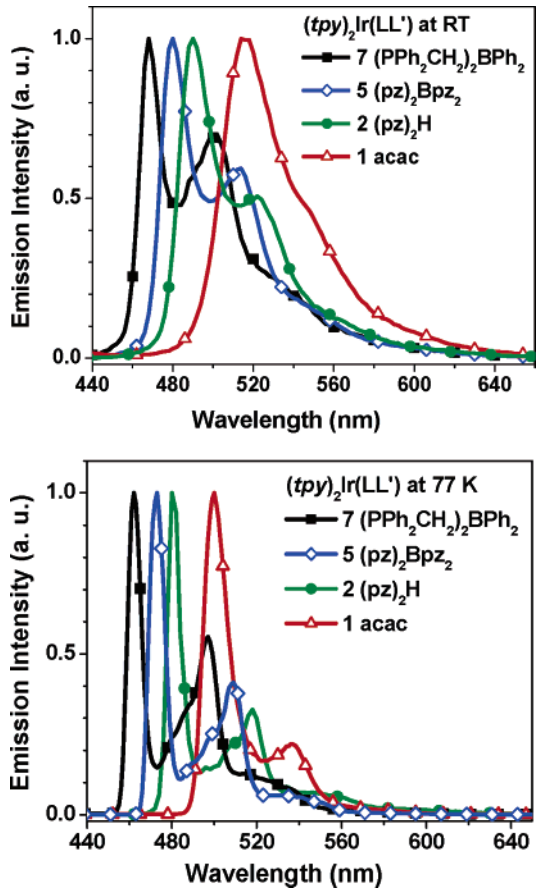

Figure 6. Room-temperature (top) and 77 K emission (bottom) spectra of $(tpy)_2Ir(PPh_2CH_2)_2BPh_2$, $(tpy)_2Ir(pz)_2Bpz_2$, $(tpy)_2Ir(pz)_2H$, and $(tpy)_2Ir$-(acac) complexes in 2-MeTHF.

The room-temperature and 77 K emission spectra of $(tpy)_2Ir(PPh_2CH_2)_2BPh_2$, $(tpy)_2Ir(pz)_2Bpz_2$, $(tpy)_2Ir(pz)_2H$, and $(tpy)_2Ir(acac)$ are shown in Figure 6. Most of the $(tpy)_2Ir$-(LL′) complexes are strongly luminescent (quantum yields (Φ) = 0.26−0.55) and have short luminescence lifetimes (τ = 2−5 μs) at room temperature, similar to values reported for *fac*-Ir$(tpy)_3$. Exceptions are complexes with diphosphine (Φ < 0.04) and isocyanide (τ = 35 μs) ligands. All of the $(tpy)_2Ir(LL')$ complexes are intensely emissive at low temperature (77 K), and most have short luminescence lifetimes (τ = 3−5 μs). Again, the complexes with diphosphine and isocyanide ligands are exceptions with τ > 23 μs. The radiative (k_r) and nonradiative decay (k_{nr}) rates can be calculated from the room-temperature Φ and τ data.[57] The k_r values of the $(tpy)_2Ir(LL')$ complexes range between 2.7 × 10^5 and 3 × 10^3 s^{-1} with the lowest values for complexes with the highest emission energy. The k_{nr} values span a narrower range of values (2.2 × 10^4 to 9.0 × 10^5 s^{-1}) and tend to decrease as the emission energy increases.

(57) The equations of $k_r = \Phi/\tau$ and $k_{nr} = (1-\Phi)/\tau$ were used to calculate the rates of radiative and nonradiative decay, where Φ is the quantum efficiency and τ is the luminescence lifetime of the sample at room temperature.

Table 5. Excited State Properties and IR Absorption of Selected $(tpy)_2Ir(LL')$ Complexes and Free *tpy*H Ligand[a]

$(tpy)_2Ir(LL')$	E_{em} (0−0) (10^6 cm^{-1})	$\hbar\omega_M$ (cm^{-1})	S_M	IR absorption (1400−1550 cm^{-1})
1 $(tpy)_2Ir(acac)$	2.00	1413	0.22	1514, 1476, 1428, 1401
2 $(tpy)_2Ir(pz)_2H$	2.08	1528	0.33	1476, 1428, 1406
5 $(tpy)_2Ir(pz)_2Bpz_2$	2.11	1495	0.41	1505, 1478, 1466, 1429, 1411, 1402
7 $(tpy)_2Ir(PPh_2CH_2)_2BPh_2$	2.16	1524	0.55	1480, 1433
12 $[(tpy)_2Ir(CN\text{-}t\text{-}Bu)_2]$ (CF_3SO_3)	2.20	1535	0.64	1508, 1482, 1466, 1432, 1402
free *tpy* ligand	2.29	1522	1.53	1514, 1467, 1433

[a] The emission energy, $E_{em}(0-0)$, was obtained from the maximum emission wavelength at 77 K. The Huang−Rhys factor, S_M, was estimated from the peak heights of the first two features of the 77 K emission spectra. The energy of $\hbar\omega_M$ was obtained from the energy difference (in cm^{-1}) of the first two emission peaks.

The structured luminescent spectra display vibronic progressions that become more highly resolved with increasing emission energy. Two prominent vibronic features are present in the emission spectra (Figure 6). The vibrational fine-structure observed in emission spectra is often the result of several overlapping satellites belonging to different vibronic transitions.[58] Here we analyze the emission spectra qualitatively and simply assume that the vibrational progression is only due to the dominant vibrational stretch. The intensity ratio of this first major vibrational transition to the highest energy peak ($E_{em}(0-0)$) is a measure of vibronic coupling between the ground and excited state (Huang−Rhys factor, S_M) and is proportional to the degree of structural distortion that occurs in the excited state relative to the ground state.[28,32,59−62] The dominant vibrational mode associated with the excited-state distortion ($\hbar\omega_M$) can be obtained from the energy difference (in cm^{-1}) of these vibronic transitions at 77 K, whereas the S_M value can be estimated from the peak heights.[60] Table 5 lists some parameters of the emission spectra (77 K) including $E_{em}(0-0)$, S_M, $\hbar\omega_M$, and selected IR absorption data for several $(tpy)_2Ir(LL')$ complexes and *tpy*H. Although all of the Ir complexes have the same "$(tpy)_2Ir$" fragment, $E_{em}(0-0)$ shifts to higher energy in complexes with stronger ligand field strength ancillary ligands such as $Ph_2B(CH_2PPh_2)_2^-$. The Huang−Rhys factors also increase monotonically with increasing $E_{em}(0-0)$, and the S_M value of *tpy*H is larger than values found for any of the $(tpy)_2Ir(LL')$ complexes.

Optical Transition Energies vs Redox Potentials. Previous investigations of diimine complexes of Ru(II) and Os(II), e.g., $Ru(bpy)_2L_2^{2+}$, have shown that absorption and emission energies increase linearly with an increase in the electrochemical gap, $\Delta E_{1/2}$ (the energy difference between the first oxidation potential and first reduction potential of the parent complex).[28] The linear relationship is consistent with the proposed model that describes formation of the MLCT state from an electronic transition between a metal-centered HOMO to ligand-localized LUMO.[27,28] For the $(tpy)_2Ir(LL')$ complexes, there is also a close correspondence between the $\Delta E_{1/2}$ values and the singlet ($E_{1_{MLCT}}$) absorption energies (Table 3). The small differences between the $\Delta E_{1/2}$ and $E_{1_{MLCT}}$ values (<0.15 eV) indicate that Franck−Condon factors contribute little to the intra- and intermolecular reorganization energies upon optical excitation. A linear correlation is obtained when the $E_{1_{MLCT}}$ and triplet (E_{T_1}) absorption energies are plotted versus $\Delta E_{1/2}$ (Figure 7). The near unity of the slope of $E_{1_{MLCT}}$ versus $\Delta E_{1/2}$ (0.84) provides further support for the assignment of $E_{1_{MLCT}}$ to a charge-transfer transition.

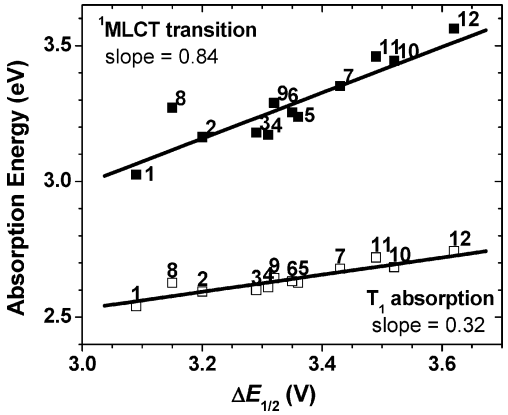

Figure 7. Plot of ^{1}MLCT absorption energy ($E_{1_{MLCT}}$, filled squares) and T_1 absorption energy (E_{T_1}, empty squares) vs electrochemical gap ($\Delta E_{1/2}$) of $(tpy)_2Ir(LL')$ complexes. The linear fits are also shown in the graph. The ancillary ligands (LL′) are numbered as in Figure 1.

To illustrate the influence the various ancillary ligands have on the HOMO and LUMO energies, the reduction (E_{red}) and oxidation potentials (E_{ox}) of the neutral $(tpy)_2Ir(LL')$ complexes are plotted separately versus E_{T_1} in Figure 8. It is apparent from the plots that nearly all the variation in triplet energy occurs from changes in the E_{ox}, not E_{red}. Likewise, the redox potentials of all the cationic $(tpy)_2Ir(LL')$ complexes (triangles in Figure 8) follow the same trends as their neutral analogues. The experimental data concur with the DFT calculation results: a LUMO localized predominantly on the pyridyl orbitals and a HOMO that is largely metal-aryl in character, in which only the HOMO is affected by the ancillary ligand. Thus, the ancillary ligands increase the optical energy gap, i.e., the $E_{1_{MLCT}}$ and T_1 absorption energies, by lowering the HOMO energy while leaving the LUMO energy relatively unchanged.

It is noteworthy that the slope of E_{T_1} versus $\Delta E_{1/2}$ (0.32) in Figure 7 is much lower than that of $E_{1_{MLCT}}$ versus $\Delta E_{1/2}$ (0.84). The difference between $E_{1_{MLCT}}$ and E_{T_1} (ΔE_{ST}) is related to the exchange energy of a complex. Large exchange energies occur when the orbitals involved with a triplet state

(58) (a) Humbs, W.; Yersin, H. *Inorg. Chim. Acta* **1997**, *265*, 139. (b) Yersin, H.; Schuetzenmeier, S.; Wiedenhofer, H.; von Zelewsky, A. *J. Phys. Chem.* **1993**, *97*, 13496.
(59) Caspar, J. V.; Westmoreland, T. D.; Allen, G. H.; Bradley, P. G.; Meyer, T. J.; Woodruff, W. H. *J. Am. Chem. Soc.* **1984**, *106*, 3492.
(60) Rillema, D. P.; Blanton, C. B.; Shaver, R. J.; Jackman, D. C.; Boldaji, M.; Bundy, S.; Worl, L. A.; Meyer, T. J. *Inorg. Chem.* **1992**, *31*, 1600.
(61) Allen, G. H.; White, R. P.; Rillema, D. P.; Meyer, T. J. *J. Am. Chem. Soc.* **1984**, *106*, 2613.
(62) Damrauer, N. L.; Boussie, T. R.; Devenney, M.; McCusker, J. K. *J. Am. Chem. Soc.* **1997**, *119*, 8253.

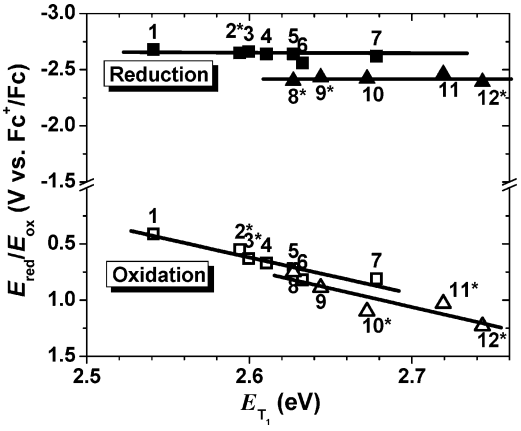

Figure 8. Plot of red/ox potentials vs emission energy, E_{em}(RT), of $(tpy)_2$Ir(LL′) complexes. The ancillary ligands (LL′) are numbered as in Figure 1. Neutral $(tpy)_2$Ir(LL′) complexes (squares) and cationic $(tpy)_2$Ir(LL′) complexes (triangles); reduction potentials (filled) and oxidation potentials (empty). The asterisk (*) indicates an irreversible oxidation or reduction process; otherwise the electrochemical process is reversible or *quasi*-reversible.

have a significant spatial overlap with those of a singlet state, whereas small exchange energies occur when the orbital overlap between the two states is poor. For example, a decrease in ΔE_{ST} is observed in linear conjugated polymers as a function of chain length in going from monomer to polymer.[63] The decrease in ΔE_{ST} with increasing chain length in the conjugated systems has been attributed to the singlet state becoming more delocalized compared to the relatively localized triplet state. By analogy, the decrease in ΔE_{ST} with decreasing $\Delta E_{1/2}$ in the $(tpy)_2$Ir(LL′) complexes implies that the ^{1}MLCT state acquires a more delocalized character with decreasing energy than does the T_1 state. Similar reductions in ΔE_{ST} with decreasing $\Delta E_{1/2}$ also occur in M$(bpy)_2L_2^{2+}$ complexes (M = Ru, Os).[27,64] The small slope of T_1 vs $\Delta E_{1/2}$ and consequent decrease in ΔE_{ST} may be due to localization of the triplet state onto a single cyclometalated ligand in the $(tpy)_2$Ir(LL′) complexes.[65]

Ground-State and Excited-State Properties. The lowest energy excited state of $4d^6$ and $5d^6$ complexes with π-accepting cyclometalating ligands can be characterized as a dominant ligand-centered $^3\pi-\pi^*$ state with some ^{1}MLCT character mixed in by spin−orbit coupling (Figure 9).[14,29,66] By applying first-order perturbation theory, the following formula can be used to define the lowest excited state (eq 4):

$$\Psi_{T_1} = \sqrt{1-\alpha^2}|^3\mathrm{LC}\rangle + \alpha|^1\mathrm{MLCT}\rangle \qquad (4)$$

where Ψ_{T_1} is the wave function of the lowest excited state and α is a coefficient that gives an estimate of the degree of singlet character mixed into the unperturbed triplet state

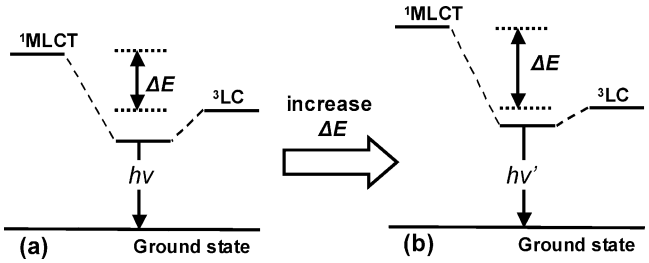

Figure 9. Schematic energy level diagram for state mixing in cyclometalated Ir(III) complexes with different ΔE: (a) small ΔE, large admixture of ^{1}MLCT and ^{3}LC, low emission energy; (b) large ΔE, small admixture of ^{1}MLCT and ^{3}LC, high emission energy.

(^{3}LC).[14] The value of α can be approximated with the formula

$$\alpha = \frac{\langle ^3\mathrm{LC}|H_{SO}|^1\mathrm{MLCT}\rangle}{\Delta E} \qquad (5)$$

where $\langle ^3\mathrm{LC}|H_{SO}|^1\mathrm{MLCT}\rangle$ is the spin−orbital coupling matrix element, characterizing the strength of spin−orbital coupling between ^{3}LC and ^{1}MLCT, and ΔE is the energy difference between the ^{3}LC and ^{1}MLCT transitions.[14] Equations 4 and 5 have been used to correlate α values with the luminescent properties of diimine and cyclometalated Rh(III) and Ir(III) complexes.[14] Only small amounts of ^{1}MLCT character need be mixed into the lowest excited state to significantly increase the ^{3}LC oscillator strength and radiative decay rate in luminescent metal complexes. For example, Güdel and coworkers have estimated that α is 0.085 in the strongly luminescent complex $(ppy)_2$Ir(bpy)$^+$.[9,14] Moreover, since α is inversely proportional to ΔE, the ΔE value can be used to evaluate the properties of the lowest excited state, provided that $\langle ^3\mathrm{LC}|H_{SO}|^1\mathrm{MLCT}\rangle$ remains invariant in the series of metal complexes. For all the $(tpy)_2$Ir(LL′) complexes, the energy level of the unperturbed ^{3}LC state can, to a first approximation, be assumed to be constant since all species have the same cyclometalating ligand. However, the energy of the ^{1}MLCT state, and likewise ΔE, will increase with increasing stability of the HOMO. Increasing ΔE decreases the amount of ^{1}MLCT character mixed into the T_1 state (Figure 9b), which in turn is expected to decrease the oscillator strength for this transition,[14] a premise that is strongly supported by our study. Ancillary ligands that increase the T_1 transition energy of the $(tpy)_2$Ir(LL′) complexes also decrease the extinction coefficient (Figure 5, Table 4). For example, the value of the T_1 extinction coefficient for $(tpy)_2$Ir$(Ph_2B(CH_2PPh_2)_2)$ is 4% that of $(tpy)_2$Ir(acac). However, the ^{1}MLCT extinction coefficients in the corresponding $(tpy)_2$Ir(LL′) complexes do not change significantly with increasing transition energy. The decrease in oscillator strength with increasing absorption energy for the T_1 transition is consistent with a lowest excited state that has less ^{1}MLCT admixture and thus, more spin-forbidden character.

For all $(tpy)_2$Ir(LL′) complexes, the increase of emission energies (E_{em}) is accompanied by an increase in the Huang−Rhys factor, S_M (shown in Table 5). The values of the vibronic spacing for all the selected $(tpy)_2$Ir(LL′) complexes

(63) (a) Köhler, A.; Beljonne, D. *Adv. Funct. Mater.* **2004**, *14*, 11. (b) Liu, Y.; Jiang, S.; Glusac, K.; Powell, D. H.; Anderson, D. F.; Schanze, K. S. *J. Am. Chem. Soc.* **2002**, *124*, 12412.
(64) Vlcek, A. A.; Dodsworth, E. S.; Pietro, W. J.; Lever, A. B. P. *Inorg. Chem.* **1995**, *34*, 1906.
(65) (a) Vacha, M.; Koide, Y.; Kotani, M.; Sato, H. *J. Luminescence* **2004**, *107*, 51. (b) Yeh, A. T.; Shank, C. V.; McCusker, J. K. *Science* **2000**, *289*, 935.
(66) Komada, Y.; Yamauchi, S.; Hirota, N. *J. Phys. Chem.* **1986**, *90*, 6425.

and *tpy*H are the same within experimental error ($\hbar\omega_M \approx 1480 \pm 90$ cm^{-1}). The dominant vibronic transition that appears in the emission spectra can be correlated with vibrational features between 1400 and 1520 cm^{-1} in the IR spectra of the corresponding $(tpy)_2$Ir(LL′) complexes and *tpy*H. The IR transitions can be assigned to C−C inter-ring stretching modes by comparison to similar vibrations identified in $[Ru(bpy)_3]^{2+}$ by normal coordinate analysis.[21,67] The S_M value quantifies the degree of electron-vibrational coupling, and large S_M values indicate strong coupling between the dominant ligand-localized vibrations in the excited and ground states.[28,59] Therefore, the increase in S_M with increasing emission energies is consistent with a T_1 state that becomes more ligand-localized (^{3}LC) in character. An alternative explanation is that an increasing ^{1}MLCT admixture expands the electronic spatial extensions, resulting in a decreased charge density per cyclometalating ligand and weaker coupling between vibrational levels in the ground and excited T_1 state.[13] Thus, this explanantion also suggests that the increase of S_M values indicates less ^{1}MLCT character in the T_1 state, i.e., the lowest excited state of the $(tpy)_2$Ir(LL′) complexes has more ^{3}LC (less delocalized) character as the T_1 energy increases.

The polarity of a molecule in an excited state is correlated to the rigidochromic shift, i.e., the energy difference of E_{em}(0−0) for dilute solutions at room temperature and 77 K.[20,68] A molecule in the excited state can reach a fully relaxed geometry upon solvent reorientation in a low-viscosity medium at room temperature, whereas the molecular excited state cannot fully relax in highly viscous, frozen media at 77 K. Thus, emission spectra from molecules with luminescent charge-transfer transitions typically display hypsochromic shifts upon going from room-temperature fluid solution to 77 K glass. A greater ^{1}MLCT character in the lowest excited state of the Ir complexes is expected to lead to greater change in the dipole moment upon excitation, resulting in larger rigidochromic shifts.[20,68] A plot of the rigidochromic shift (ν_{max}(77 K) − ν_{max}(RT)) versus E_{em}(RT) for the $(tpy)_2$Ir(LL′) complexes in 2-MeTHF (Figure S4, see also Table 4) shows an increase with decreasing emission energies, consistent with the proposed increase in ^{1}MLCT character with decreasing T_1 state energy.

The ancillary ligands of the $(tpy)_2$Ir(LL′) complexes significantly affect the luminescent quantum yield. Since Φ is dependent on both the radiative and nonradiative decay rates,[69] the k_r and k_{nr} values need to be considered individually in order to determine the overall influence on Φ brought about by the ancillary ligands. Previous investigations of Ru(II) and Os(II) polypyridyl complexes have shown that the Φ values for these species are dictated by the variation in k_{nr} with energy. The k_{nr} values for a large number of luminescent diimine transition complexes have also been

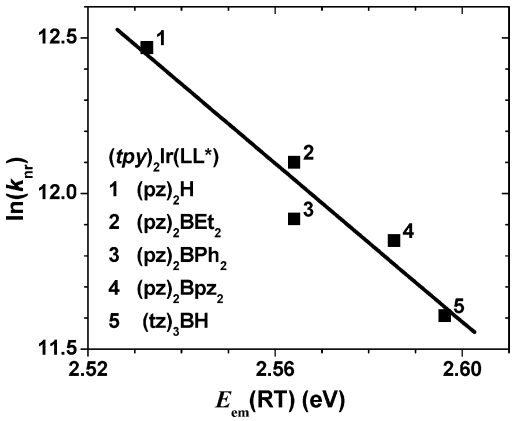

Figure 10. Plot of nonradiative decay rate (ln(k_{nr})) vs emission energy (E_{em}(RT)) for neutral $(tpy)_2$Ir(LL*) (LL* = pyrazolyl ligands) complexes.

shown to follow the energy gap law for radiationless transitions.[28,59−62] A linear decrease between ln(k_{nr}) with increasing emission energy is deduced from the energy gap law if the dominant radiationless process is assigned to the same vibrational states in closely related systems. For the $(tpy)_2$Ir(LL′) complexes, the k_{nr} values decrease with increasing E_{em}(RT). A linear relationship of ln(k_{nr}) vs E_{em}(RT) is obtained for the series of neutral $(tpy)_2$Ir(LL*) complexes (Figure 10), where the Ir complexes considered here retain a similar "$(tpy)_2$Ir$(pz)_2$" core. Since the k_{nr} values for the $(tpy)_2$Ir(LL′) complexes also appear to follow the energy gap law, any decrease in Φ with increasing emission energy cannot be attributed to an increase in nonradiative decay rate. In particular, the low Φ values of the $(tpy)_2$Ir(LL′) complexes with diphosphine ligands are mostly due to their small respective k_r values, since their k_{nr} values are similar to rates found in other $(tpy)_2$Ir(LL′) complexes with much larger values of Φ.

The radiative rates of the $(tpy)_2$Ir(LL′) complexes decrease with increasing emission energies (Table 4).[70] The k_r values for $(tpy)_2$Ir(LL′) complexes with E_{em}(RT) < 2.65 eV are ca. 10^5 s^{-1}, comparable to values found in Os(II) polypyridyl complexes,[61] whereas k_r values decrease to $<10^4$ s^{-1} for the $(tpy)_2$Ir(LL′) complexes with E_{em}(RT) > 2.65 eV. The radiative decay rate can be related to the emission energy using eq 6:

$$k_r = \frac{4E_{em}^{\ 3}}{3\hbar} |\langle\psi_e|\vec{d}|\psi_g\rangle|^2 \qquad (6)$$

where $|\langle\psi_e|\vec{d}|\psi_g\rangle|^2$ describes the probability for an excited- to ground-state transition.[28,71,72] In an investigation of Os-

(67) (a) Finkenzeller, W.; Stoessel, P.; Kulikova, M.; Yersin, H. *Proceedings of SPIE "Optical Science and Technology"*, San Diego (USA), August **2003**, (*Conference 5214*). (b) Strommen, D. P.; Mallick, P. K.; Danzer, G. D.; Lumpkin, R. S.; Kincaid, J. R. *J. Phys. Chem.* **1990**, *94*, 1357.
(68) Cummings, S. D.; Eisenberg, R. *J. Am. Chem. Soc.* **1996**, *118*, 1949.
(69) $\Phi = k_r/(k_r + k_{nr})$.
(70) For comparative purposes the radiative decay rates (k_r) of compounds **13** and **14** given in Table 4 are from data measured in degassed 2-MeTHF solution. The absorption spectra and extinction coefficients of **13** and **14** (in CH_2Cl_2) and room-temperature luminescence lifetimes ($\tau = 1.5$ μs for **13** and $\tau = 2.9$ μs for **14** in degassed CH_3CN) are comparable to the reported data in ref 18. However, the quantum efficiencies we measure for these Ir complexes are significantly lower than the reference data.
(71) Herzberg, G. *Molecular Spectra and Molecular Structure*; Van Nostrand: New York, 1950; Vol. 1, Chapter 4.
(72) Turro, N. J. *Modern Molecular Photochemistry*; University Science Books: Mill Valley, CA, 1978; pp 86−88.

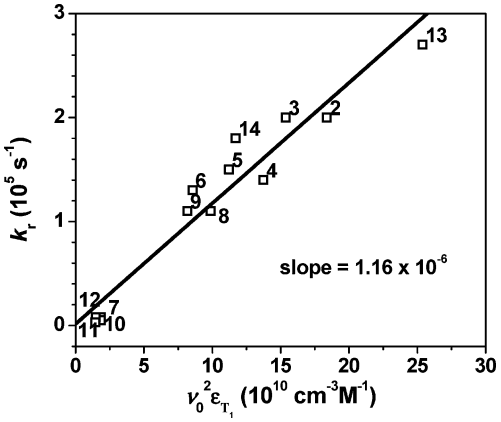

Figure 11. Plot of k_r vs $\nu_0^2\epsilon_{T_1}$ for $(tpy)_2$Ir(LL′) complexes. The ancillary ligands (LL′) are numbered as in Figure 1 (k_r = rate of radiative decay, ν_0 and ϵ_{T_1} = T_1 absorption energy and extinction coefficient, respectively).

(II) polypyridyl complexes, Meyer et al. assumed a constant value of $|\langle\psi_e|\vec{d}|\psi_g\rangle|^2$ for all complexes studied and noted a roughly linear increase in k_r with an increase in E_{em}.[3,61] However, since k_r decreases with increasing E_{em}(RT) in the $(tpy)_2$Ir(LL′) complexes, the transition probability for these cyclometalated species must be decreasing with increasing E_{em}(RT).

According to classical theory,[61,72] the radiative decay rate for emission can be related to the oscillator strength (*f*) for absorption, provided that the absorption and emission transitions involve the same initial and final states. The oscillator strength is proportional to the width of the absorption band at $^1/_2\epsilon_{max}(\Delta\nu_{1/2})$ for transitions with a Gaussian line shape. Equation 7 can then be used to calculate k_r using the intensity of the corresponding absorption band:

$$k_r = 3 \times 10^{-9}\, \nu_0^{\,2} \int \epsilon \, d\nu \approx 3 \times 10^{-9}\, \nu_0^{\,2} \epsilon \Delta\nu_{1/2} \qquad (7)$$

where ν_0 is the energy (in cm^{-1}) corresponding to the maximum wavelength of absorption and $\int\epsilon\, d\nu$ is the area of the molecular extinction coefficient.[72] The distinctive T_1 absorption bands displayed by the $(tpy)_2$Ir(LL′) complexes (Figure 5, inset) are in contrast to the broad, ill-defined bands that are observed for similar transitions in Os(II) and Ru(II) polypyridyl complexes.[28] The well-resolved T_1 absorption transition allows for an accurate assessment of ϵ. However, for $(tpy)_2$Ir(acac), the T_1 absorption band is overlapped with higher energy MLCT transitions, which precludes accurate identification of ϵ; therefore, this complex was not included in the following analysis. A plot of k_r versus $\nu_0^2\epsilon$ for complexes **2**−**14** is shown in Figure 11. The good linear fit between k_r and $\nu_0^2\epsilon_{T_1}$ is consistent with emission originating from a common state, i.e., the "$(tpy)_2$Ir" fragment. A $\Delta\nu_{1/2}$ value of 410 cm^{-1} is derived from the slope of the plot, which is comparable to the line width reported for the lowest triplet transition in $[Os(bpy)_3]^{2+}$ (300 cm^{-1} at 5 K).[73] Therefore, the absorption properties of the T_1 band reflect the luminescent characteristics and can be used to evaluate the emission properties of the respective $(tpy)_2$Ir(LL′) complexes.

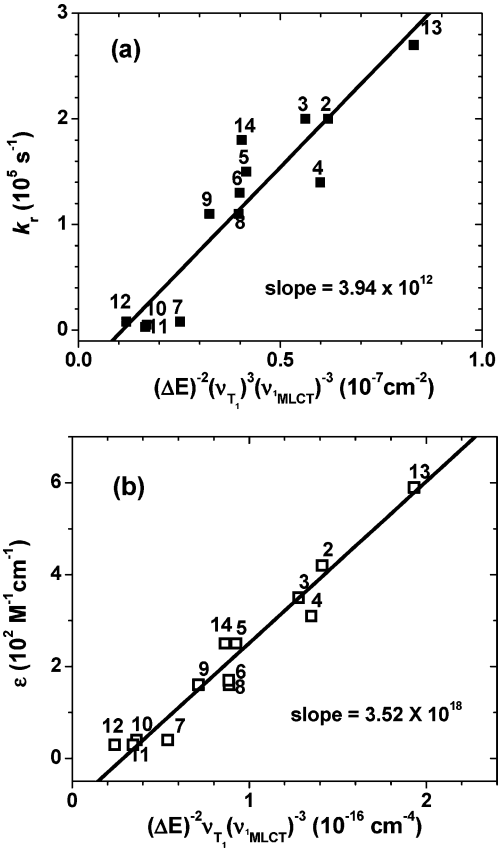

Figure 12. (a) Plot of radiative decay rate (k_r) vs $(1/\Delta E)^2(\nu_{T_1}/\nu_{1_{MLCT}})^3$ for $(tpy)_2$Ir(LL′) complexes. (b) Plot of ϵ vs $(1/\Delta E)^2(\nu_{T_1}/\nu_{1_{MLCT}}{}^3)$. The ancillary ligands (LL′) are numbered as in Figure 1.

The oscillator strength and consequently k_r are dependent on the amount of ^{1}MLCT character that is mixed into the T_1 state which, in turn, depends on ΔE. It is possible to calculate k_r as a function of ΔE using eq 8.[58,74]

$$k_r = k_r(^1\mathrm{MLCT})\left(\frac{\langle {}^3\mathrm{LC}|H_{SO}|{}^1\mathrm{MLCT}\rangle}{\Delta E}\right)^2\left(\frac{\nu_{T_1}}{\nu_{1_{MLCT}}}\right)^3 \qquad (8)$$

Here, $k_r(^1$MLCT) is the radiative rate of the perturbing state while ν_{T_1} and $\nu_{1_{MLCT}}$ are the respective absorption transition energies. The $k_r(^1$MLCT) value can be considered essentially constant since the magnitude is proportional to the oscillator strength of the ^{1}MLCT transition, which is roughly the same for all the complexes. Values for ΔE can be obtained from the $\nu_{1_{MLCT}}$ data and by using the emission energy of $(ppy)_2$Pt-(CH_2Cl)Cl (444 nm, 22500 cm^{-1}, $k_r = 10^3$ s^{-1}) as the ^{3}LC energy for an unperturbed "$(tpy)_2$Ir" fragment, since the Pt-(IV) complex has a ligand-centered excited state perturbed only by metalation to the heavy atom.[85] On the basis of eq 8, k_r values should be linearly proportional to $(1/\Delta E)^2(\nu_{T_1}/\nu_{1_{MLCT}})^3$, provided that $\langle {}^3\mathrm{LC}|H_{SO}|{}^1\mathrm{MLCT}\rangle$ is constant (Figure 12a). Alternatively, eqs 7 and 8 can be combined and

(73) (a) Felix, F.; Ferguson, J.; Güdel, H. U.; Ludi, A. *Chem. Phys. Lett.* **1979**, *62*, 153. (b) Decurtins, S.; Felix, F.; Ferguson, J.; Güdel, H. U.; Ludi, A. *J. Am. Chem. Soc.* **1980**, *102*, 4102.

(74) McGlynn, S. P.; Azumi, T.; Kinoshita, M. *Molecular Spectroscopy of the Triplet State*; Prentice Hall: Englewood Cliffs, NJ, 1969; Chapter 5.

Table 6. Photophysical Properties of $(dfppy)_2Ir(LL')$ Complexes[a]

		emission at RT					emission at 77 K	
$(C\wedge N)_2Ir(LX)$	abs, λ_{max} λ(nm) $\{\epsilon, 10^3 cm^{-1}M^{-1}\}$	λ_{max} (nm)	τ (μs)	Φ_{PL}	k_r 10^5 s^{-1}	k_{nr} 10^5 s^{-1}	λ_{max} (nm)	τ (μs)
1 $(dfppy)_2Ir(acac)$	254 (47.8), 387 (5.0), 461 (0.9)	482	1.2	0.62	5.2	3.2	469	2.8
2 $(dfppy)_2Ir(pz)_2H$	253 (42.3), 323 (11.8), 375 (5.3), 456 (0.4)	466	1.5	0.62	4.1	2.5	458	2.4
5 $(dfppy)_2Ir(pz)_2Bpz_2$	252 (39.8), 367 (4.9), 420 (0.52), 451(0.22)	456	3.7	0.73	2.0	0.73	450	4.0
7 $(dfppy)_2Ir(PPh_2CH_2)_2BPh_2$	251 (51.5), 312 (13.8), 413 (0.1), 442 (0.04)	448	8.4	0.19	0.22	1.0	443	19.7
12 $[(dfppy)_2Ir(CN\text{-}t\text{-}Bu)_2](CF_3SO_3)$	252 (44.9), 308 (20.1), 412 (0.1), 440 (0.06)	444 (sh), 468	6.2	0.16	0.26	1.4	442	7.8

[a] The absorption spectra were measured in CH_2Cl_2 and the emission spectra were measured in 2-MeTHF solution.

rearranged to give eq 9.

$$\epsilon = k_r(^1\text{MLCT})\left(\frac{1}{3\times 10^{-9}\,\Delta\upsilon_{1/2}}\right)\left(\frac{\langle ^3\text{LC}|H_{SO}|^1\text{MLCT}\rangle}{\Delta E}\right)^2\left(\frac{\nu_{T_1}}{\nu_{1_{MLCT}}{}^3}\right) \quad (9)$$

The derivation used to generate eq 9 is similar to the approach used by Demas and Crosby to correlate ^{1}MLCT and T_1 energies of Ru and Os polypyridyl complexes to extinction coefficients and radiative rates.[75] The analysis has also been shown by Watts to be applicable to both cyclometalated and polypyridyl Ir complexes.[4,76,77] Equation 9 has the advantage of using only absorption data to generate a plot. Thus, on the basis of eq 9, a linear fit of ϵ vs $(1/\Delta E)^2$-$(\nu_{T_1}/\nu_{1_{MLCT}}{}^3)$ can also be used to derive a value of $\langle ^3\text{LC}|H_{SO}|^1$-MLCT$\rangle$ for the $(tpy)_2Ir(LL')$ complexes (Figure 12b). If one assumes that $k_r(^1\text{MLCT})$ has the same value as for $[Ru(bpy)_3]^{2+}$ ($\sim 10^8$ s^{-1}),[78] a value of 200 cm^{-1} is obtained for $\langle ^3\text{LC}|H_{SO}|^1\text{MLCT}\rangle$ from the slopes of Figure 12a,b (using a value of 410 cm^{-1} for $\Delta\nu_{1/2}$ in eq 9). Interestingly, the $\langle ^3\text{LC}|H_{SO}|^1\text{MLCT}\rangle$ value estimated from such an analysis of room-temperature data is intermediate between $\langle ^3\text{LC}|H_{SO}|^1$-MLCT$\rangle$ values determined for the cyclometalated complexes $(ppy)_2Ir(bpy)^+$ (147 cm^{-1}) and $(thpy)_2Ir(bpy)^+$ (237 cm^{-1}) ($thpy$ = 2-(2-thienyl)pyridyl) using low-temperature, high-resolution spectroscopy.[14] A close inspection of the data (Table S1) also reveals that variation in k_r and ϵ in Figure 12a,b, respectively, is most strongly correlated by the nearly 5-fold change in the ΔE^{-2} term. Therefore, the decrease in the k_r (and ϵ) values with increasing emission energy can be ascribed to an increase in the ^{1}MLCT transition energy, and likewise ΔE, brought about by a decrease in the HOMO energy, which leads to less mixing of ^{1}MLCT character into the lowest T_1 state.

A large decrease in k_r values in both the CN-*t*-Bu and $(PPh_2CH_2)_2BPh_2^-$ based $(tpy)_2Ir(LL')$ complexes can also be correlated with an increase in the Ir$-C_{aryl}$ bond lengths. The Ir$-C_{aryl}$ bonds are longer than the corresponding bonds in $(tpy)_2Ir(acac)$ due to the relatively stronger *trans* influence of the two types of ancillary ligands. The longer Ir$-C_{aryl}$ bonds are expected to influence the metal−ligand stretching vibrations, which also play a role in the vibronic coupling between the excited and ground states (Herzberg−Teller coupling).[12] Thus, in addition to the decline in k_r caused by an increase in ΔE, the isocyanide and phosphino ligands may decrease the coupling between the ground and excited states by weakening the Ir$-C_{aryl}$ bonds, resulting in a further decrease in k_r values.

A smaller series of $(dfppy)_2Ir(LL')$ complexes were examined using a related set of ancillary ligands (Table 6). Substituting fluorine in the 4′,6′-positions of the 2-phenylpyridyl ligand leads to a hypsochromic shift in the emission spectra relative to their $(tpy)_2Ir(LL')$ analogues, as expected from results obtained with related tris-cyclometalated complexes.[16,19] The higher triplet energy of *dfppy* relative to *tpy* leads to both a decrease in k_{nr} (energy gap law) and an increase in k_r (eq 6) resulting in higher Φ values for the $(dfppy)_2Ir(LL')$ derivatives. The $(dfppy)_2Ir(LL')$ complexes display a decrease in k_r with increasing emission energy similar to that observed in the $(tpy)_2Ir(LL')$ complexes, suggesting that the effects of ancillary ligands on the excited-state properties of Ir complexes are independent of the choice of cyclometalating ligand. The fact that the same ancillary ligands decrease k_r values in both types of cyclometalated species supports the proposal that the low k_r values are caused by a decrease in the HOMO energy and consequently an increase in ΔE, that decreases the amount of ^{1}MLCT character mixed into the T_1 state.

Conclusion

The photophysical and electrochemical properties of a series of $(tpy)_2Ir(LL')$ complexes have been examined. The studies presented here demonstrate that it is possible to tune the properties of the lowest excited state chemically by only employing different ancillary ligands. The ancillary ligands increase the optical energy gap of Ir complexes by lowering the HOMO (related to the oxidation of metal-centered orbitals) and leave the LUMO (related to the reduction of ligand-localized orbitals) unchanged. The destabilization of the ^{1}MLCT state results in a decreased ^{1}MLCT character in the lowest excited state, thereby increasing the lowest excited state energy. In addition, the reduced ^{1}MLCT character within the lowest excited state has pronounced effects on the photophysical properties of the Ir complexes: the excited states become more ligand-localized with stronger coupling with the dominant vibrational mode, the oscillator strength of the T_1 transition decreases, and the decreased ^{1}MLCT admixture leads to a decrease in radiative decay rates.

(75) Demas, J. N.; Crosby, G. A. *J. Am. Chem. Soc.* **1971**, *93*, 2841.
(76) Watts, R. J.; Crosby, G. A. *J. Am. Chem. Soc.* **1972**, *94*, 2606.
(77) Watts, R. J.; Crosby, G. A.; Sansregret, J. L. *Inorg. Chem.* **1972**, *11*, 1474.

Most of the neutral Ir complexes reported here are highly emissive at room temperature and stable to sublimation, making them ideal for use as emissive dopants in blue and white phosphorescent OLEDs. Devices fabricated using films doped with $(dfppy)_2Ir(pz)_2Bpz_2$ have external quantum efficiencies of >11% for blue phosphorescent OLEDs[79] and >12% for white phosphorescent OLEDs.[80] We are examining other related complexes as emissive dopants in monochromatic and white OLEDs. The tetrakis(pyrazolyl)borate ligand also offers the possibility of expanded coordination,[81,82] since the noncoordinated pyrazoles of $(tpy)_2Ir(pz)_2Bpz_2$ can be used to bind a second metal center. Related dinuclear organometallic complexes have been reported for Pd and Ru complexes but not, thus far, for photoactive metal fragments such as the Ir complexes reported here. The ability to make homometallic and heterometallic complexes of this type may lead to further applications for cyclometalated Ir complexes, such as photosensitizers[83] and donor−acceptor dyads.[84]

Acknowledgment. The authors thank the Universal Display Corporation, the Defense Advanced Research Projects Agency, and the National Science Foundation for their financial support.

Supporting Information Available: The UV−vis absorption and emission spectra for selected $(dfppy)_2Ir(LL')$ complexes (Figures S5−S7); the absorption spectra of $(tpy)_2Ir(pz)_2Bpz_2$ in different solvents at room temperature (Figure S2); the absorption, excitation (77 K), and emission spectra (77 K) of $(tpy)_2Ir(CN\text{-}t\text{-}Bu)_2(CF_3SO_3)$ in 2-MeTHF (Figure S3); plot of rigidochromic shifts vs emission energies for $(tpy)_2Ir(LL')$ complexes in 2-MeTHF (Figure S4); the electrochemical and photophysical properties of all $(dfppy)_2Ir(LL')$ complexes examined here (Tables S2−S4). Also included are tables of crystal data, atomic coordinates, bond distances, bond angles, and anisotropic displacement paramenters for $(tpy)_2Ir(PPh_2CH_2)_2BPh_2\cdot H_2O$ and $(tpy)_2Ir(CN\text{-}t\text{-}Bu)_2(CF_3SO_3)\cdot CHCl_3$, as well as the corresponding CIF files. This material is available free of charge via the Internet at http://pubs.acs.org.

IC048599H

(78) Yamauchi, S.; Komada, Y.; Hirota, N. *Chem. Phys. Lett.* **1986**, *129*, 197.
(79) (a) Holmes, R. J.; D'Andrade, B. W.; Forrest, S. R.; Ren, X.; Li, J.; Thompson, M. E., *Appl. Phys. Lett.* **2003**, *83*, 3818. (b) Ren, X.; Li, J.; Holmes, R. J.; Djurovich, P. I.; Forrest, S. R.; Thompson, M. E. *Chem. Mater.* **2004**, *16*, 4743.
(80) D'Andrade, B. W.; Holmes, R. J.; Forrest, S. R. *Adv. Mater.* **2004**, *16*, 624.
(81) Ruiz, J.; Florenciano, F.; Rodríguez, V.; de Haro, C.; Lopóz, G.; Pérez, J. *Eur. J. Inorg. Chem.* **2002**, 2736.
(82) Huang, L.; Seward, K. J.; Sullivan, B. P.; Jones, W. E.; Mecholsky, J. J.; Dressick, W. J. *Inorg. Chim. Acta* **2000**, *310*, 227.
(83) (a) Subhan, M. A.; Suzuki, T.; Kaizaki, S. *J. Chem. Soc., Dalton Trans.* **2002**, 1416. (b) Sanada, T.; Suzuki, T.; Yoshida, T.; Kaizaki, S. *Inorg. Chem.* **1998**, *37*, 4712. (c) Klink, S. I.; Keizer, H.; van Veggel, F. C. J. M. *Angew. Chem., Int. Ed.* **2000**, *39* (23), 4319.
(84) Kercher, M.; Konig, B.; Zieg, H.; De Cola, L. *J. Am. Chem. Soc.* **2002**, *124*, 1154.
(85) Chassot, L.; von Zelewsky, A.; Sandrini, D.; Maestri, M.; Balzani, V. *J. Am. Chem. Soc.* **1986**, *108*, 6084.